Marine and Petroleum Geology 128 (2021) 104995

Contents lists available at ScienceDirect

Marine and Petroleum Geology

journal homepage: www.elsevier.com/locate/marpetgeo

Oil and gas seepage offshore Georgia (Black Sea) – Geochemical evidences for a paleogene-neogene hydrocarbon source rock

Thomas Pape [a,*], Martin Blumenberg [b], Anja Reitz [c], Georg Scheeder [b], Mark Schmidt [c], Matthias Haeckel [c], Valentina N. Blinova [d,e], Michael K. Ivanov [d,1], Heiko Sahling [a,1], Klaus Wallmann [c], Gerhard Bohrmann [a]

[a] MARUM – Center for Marine Environmental Sciences and Faculty of Geosciences, University of Bremen, Klagenfurter Strasse 4, D-28334 Bremen, Germany
[b] BGR – Federal Institute for Geosciences and Natural Resources, Stilleweg 2, D-30655 Hannover, Germany
[c] GEOMAR Helmholtz Centre for Ocean Research Kiel, Wischhofstr. 1-3, D-24148 Kiel, Germany
[d] UNESCO MSU Center for Marine Geology and Geophysics, Faculty of Geology, Moscow State University, Vorobjevy Gory, Moscow, 119899, Russia
[e] Royal Dutch Shell, Geology and Geophysics Lead Russia, Moscow, Russia

ARTICLE INFO

Keywords:
Black sea
Seafloor seepage
Oil
Gas
Methane
Gas hydrate
Maikop group
Kuma formation

ABSTRACT

Numerous hydrocarbon seep sites at the continental shelf, slope, and in the deep water basin are known to feed the Black Sea water reservoir of dissolved methane. In this study, we identified the likely sources of gas and oil that are emitted at four sites located on the continental slope offshore Georgia in the Eastern Black Sea at 830 to 1,140 m water depth – an area with gas seepage only (Batumi seep area) and three areas of coupled gas and oil seepage (Iberia Mound, Colkheti Seep, and Pechori Mound). The geochemistry of bulk parameters, organic fractions and individual hydrocarbon biomarkers in near-surface sediments and of gas/oil expelled from the seafloor was analyzed and jointly interpreted to assign most likely hydrocarbon source rocks in the studied region. Presence of oleanane in shallow oil-impregnated sediments and oil slicks attests that the source rock at all sites is younger than Mid Cretaceous in age. We conclude that hydrocarbons ascending at all the four seepage areas originate from the Eocene Kuma Formation and/or the Oligocene–Lower Miocene Maikop Group, which are considered the principal hydrocarbon sources in the Eastern Black Sea region. Distributions of crude oil biomarkers in shallow sediments suggests moderate to heavy biodegradation. C_1/C_{2+} ratios (10–4,163) along with stable C and H isotopic ratios ($\delta^{13}C$–CH_4 −46.3 to −53.1.3‰ V-PDB; $\delta^{2}H$–CH_4 −159 to −178‰ V-SMOW) indicate gas mixtures of oil-associated thermogenic and secondary microbial light hydrocarbons that are discharged from the four seep sites. Light hydrocarbons discharged at the Batumi Seep area are characterized by significant enrichments of methane, but have almost similar $\delta^{13}C$–CH_4 values if compared to the other study sites. Such methane enrichments likely result from a comparably higher degree of petroleum degradation and associated formation of secondary microbial methane.

1. Introduction

The Black Sea basin hosts about 12 km thick, partially organic-rich sediments, which promote oil and gas formation in the deep subsurface. At numerous sites, oil and gas migrate towards the sediment surface and escape into the water body. Seafloor seepage of light hydrocarbons and partially of oil is widely distributed on Black Sea continental shelves and slopes (e.g., Artemov et al., 2007; Bohrmann et al., 2003, Bohrmann et al., 2007, 2011; Dembicki, 2020; Dimitrov, 2002; Greinert et al., 2006; Klaucke et al., 2006; Körber et al., 2014; Kruglyakova et al., 2004; Michaelis et al., 2002; Naudts et al., 2006; Nikolovska et al., 2008; Reitz et al., 2011; Riboulot et al., 2018; Römer et al., 2012, 2020; Sahling et al., 2009; Schmale et al., 2005; Zander et al., 2020, this issue). At seepage sites located within the gas hydrate stability zone (GHSZ), which at current water temperature and salinity is located in waters deeper than about 720 m below sealevel (bsl) (Naudts et al., 2006; Pape et al., 2010), concentrations of methane and other light hydrocarbons exceeding solubility lead to gas hydrate formation in

* Corresponding author.
E-mail address: tpape@marum.de (T. Pape).
[1] deceased.

https://doi.org/10.1016/j.marpetgeo.2021.104995
Received 22 August 2019; Received in revised form 4 October 2020; Accepted 21 February 2021
Available online 26 February 2021

the sediment (Vassilev and Dimitrov, 2002). Gas seepage and decomposing gas hydrates are considered the dominant source of methane in Black Sea waters, which are the world's largest aquatic reservoir of methane (96 Tg; Kessler et al., 2006; Reeburgh et al., 1991). Highest methane concentrations (up to 15 μM) are found in the permanently anoxic water body present below approx. 150 m below sea level (mbsl) (Reeburgh et al., 1991; Schmale et al., 2011).

Prominent seepage sites are situated within the GHSZ offshore Georgia, which is the area of investigation in this study. In this area, hydrocarbon upward migration is mainly related to uplift due to active tectonic compression caused by the northward movement of the Arabian plate against Eurasia (Adamia et al., 2010; Banks et al., 1997). For the Batumi seep area, hydroacoustic investigations in the water column, visual seafloor inspections and seafloor sampling have shown that it is characterized by sustained strong gas emissions and elevated methane concentrations in shallow sediments (Heeschen et al., 2011; Klaucke et al., 2006; Nikolovska et al., 2008; Pape et al., 2011; Reitz et al., 2011). Seafloor oil release was observed at other seep sites, such as the Iberia Mound, the Colkheti Seep and the Pechori Mound (Akhmetzhanov et al., 2007; Bohrmann et al., 2007, 2011; Dembicki, 2020; Körber et al., 2014; Reitz et al., 2011). The hydrocarbons nourish microbial communities thriving in sediments and the water column where they mediate the anaerobic oxidation of methane (AOM) (e.g., Blumenberg et al., 2004; Michaelis et al., 2002; Treude et al., 2007; Wakeham et al., 2007) and potentially of higher homologues (Formolo et al., 2004; Head et al., 2003; Kniemeyer et al., 2007; Stagars et al., 2016).

The Oligocene–Lower Miocene organic-rich Maikop Group, which is a potential hydrocarbon source rock in the Black Sea and the adjacent Caspian Sea (e.g., Abrams and Narimanov, 1997; Boote et al., 2018; Burwicz and Haeckel, 2020; Efendiyeva, 2004; Inan et al., 1997; Mayer et al., 2018a; 2018b; Pupp et al., 2018; Ross and Degens, 1974; Sachsenhofer et al., 2017; 2018b), was previously discussed as major source of light hydrocarbons for most of the seeps offshore Georgia (Klaucke et al., 2006; Pape et al., 2010; Reitz et al., 2011; Dembicki 2020). However, other organic-rich strata that under- and overly the Maikop Group could also account for hydrocarbon formation in the Eastern Paratethyan region. A prolific hydrocarbon source rock is the Middle Eocene Kuma Formation (Beniamovski et al., 2003; Boote et al., 2018; Mayer et al., 2018b; Pupp et al., 2018; Sachsenhofer et al., 2018a), which is also an excellent source rock in western Georgia (Vincent and Kaye, 2018). In the southern Rioni foreland basin onshore Georgia, both formations are partly buried by several kilometer-thick sediments (e.g., Tari et al., 2018). However, due to intense tectonic folding they might also reach much shallower depths in the study area (Tari and Simmons, 2018). Moreover, general assignments of formation depths for individual compound classes are difficult, since thermal gradients are variable in that region (Minshull and Keddie, 2010). Therefore, factors controlling oil and gas seepage at Pechori Mound, Colkheti Seep and Iberia Mound and the exclusive seepage of gas at the Batumi seep area are not well understood, so far.

The origin of light hydrocarbons can be assessed based on the gas molecular composition and stable isotope signatures of individual components (e.g., Berner and Faber, 1988; Faber et al., 2015; Milkov and Etiope, 2018; Pape et al., 2020, this issue; Whiticar, 1999). While microbial production leads to the almost exclusive formation of methane at relatively shallow depth and low temperatures, thermogenic production in deeper sediments and at elevated temperatures results in the concurrent formation of methane and higher hydrocarbons (e.g., Bernard et al., 1977; Claypool and Kvenvolden, 1983; Quigley and Mackenzie, 1988; Seewald, 2003). Moreover, information on the type of organic matter that is transformed into heavy hydrocarbons is gained from migrated petroleum compounds impregnating shallow sediments and fluids expelled from the seafloor (e.g., Peters et al., 2004).

In order to characterize the origin and fate of hydrocarbons transported from the deep subsurface at the four oil and gas seep sites, we combined state-of-the art sediment and gas sampling with classical organic geochemical approaches. Molecular and isotopic compositions of bulk hydrocarbon fractions, aliphatic C_{15+} hydrocarbons, tetra- and pentacyclic isoprenoidal biomarkers, and C_1–C_5 hydrocarbons from deep-sea samples were examined in detail. Joint interpretation of data obtained allowed evaluating the depositional environment, relative ages, and maturities of the organic-rich deposits that fuel hydrocarbons bound in shallow hydrates and escape the seafloor. Furthermore, volatile hydrocarbons in shallow sediments and C_{15+} hydrocarbons in natural sea surface oil slicks above one of the seep sites were evaluated with respect to potential modifications during migration through the sediment and passage through the water column. These data are useful for future explorations at these seepage sites and similar geological settings and might be of prime interest for a better understanding of deep active hydrocarbon systems in the area.

2. Geological, sedimentological and geochemical setting

2.1. Tectonic evolution of the Black Sea and of the study region

The Black Sea is thought to have formed as a Cretaceous-Paleogene back-arc basin due to extension associated with northward dipping subduction of the Paratethys oceanic plate under the Eurasian plate (Cloetingh et al., 2003; Nikishin et al., 2003; Monteleone et al., 2019; Robinson et al., 1996; Shillington et al., 2008; Zonenshain and Pichon, 1986). Several phases of compression and extension have affected the broader Black Sea region since the Cretaceous (e.g., Robinson, 1997; Nikishin et al., 2015a, 2015b; Stephenson and Shellart, 2010; Vincent et al., 2016). Nowadays, it has a maximum water depth of ca. 2,200 m and consists of two sub-basins, the Western and the Eastern Black Sea (Fig. 1a), which are separated by the central NW–SE-trending Mid-Black Sea High (Nikishin et al., 2003, 2015a; Shillington et al., 2018; Starostenko et al., 2004; Stephenson and Schellart, 2010).

The relative timing of the opening of the two Black Sea basins is still under debate (e.g., Monteleone et al., 2019 and references cited therein), but the Eastern Black Sea basin is generally considered to be younger than its Western counterpart. For a discussion about the various models regarding the age of the Eastern Black Sea, the reader is referred to Tari and Simmons (2018). Montelone et al. (2019) proposed that the Paleocene to Oligocene deposits present in the Eastern Black Sea, which harbors the study sites (Fig. 1a), record the time spanning from the initiation of breakup (Late Cretaceous-Paleocene) to the end of extension.

Because of the ongoing collision of Eurasia with the Africa-Arabian lithospheric plates since the Eocene/Oligocene, the extensional basin of the Black Sea nowadays is surrounded by large compressional structures such as the Crimean Mountains, the Caucasus, and the Pontides (e.g., Boote et al., 2018; Nikishin et al., 2015b; Okay et al., 1994). The continental slope offshore Georgia (Fig. 1a) is bordered by several structural elements like the Eastern Pontides thrust belt including the E–W trending Adjara-Trialet-Fold Belt, the east-southeast trending Greater Caucasus Thrust-Fold Belt, and the Shatsky Ridge (Adamia et al., 2010; Banks et al., 1997; Robinson, 1997; Robinson et al., 1996; Tari et al., 2018). Onshore west Georgia, the Greater Caucasus Thrust-Fold Belt and the Adjara-Trialet-Fold Belt are separated by the Rioni foreland basin, which is a molasse basin with several kilometer thick Late Miocene–Quaternary deposits mostly transported in the course of the Greater Caucasus uplift (Adamia et al., 2010; Tari et al., 2018; Vincent et al., 2007).

Subsidence promoting deposition of sediment packages of up to 12 km in thickness occurred in the central Black Sea basin probably since the Late Cretaceous/Paleocene (Cloetingh et al., 2003; Nikishin et al., 2003; Okay et al., 1994). For the Gurian thrust-fold belt (or Gurian trough), which hosts the sites studied herein, relatively thick Middle and Late Miocene deposits were interpreted to reflect the main subsidence phases (Nikishin et al., 2015a). From Middle Miocene to Pliocene sediment packages having accumulated in the Gurian trough experienced

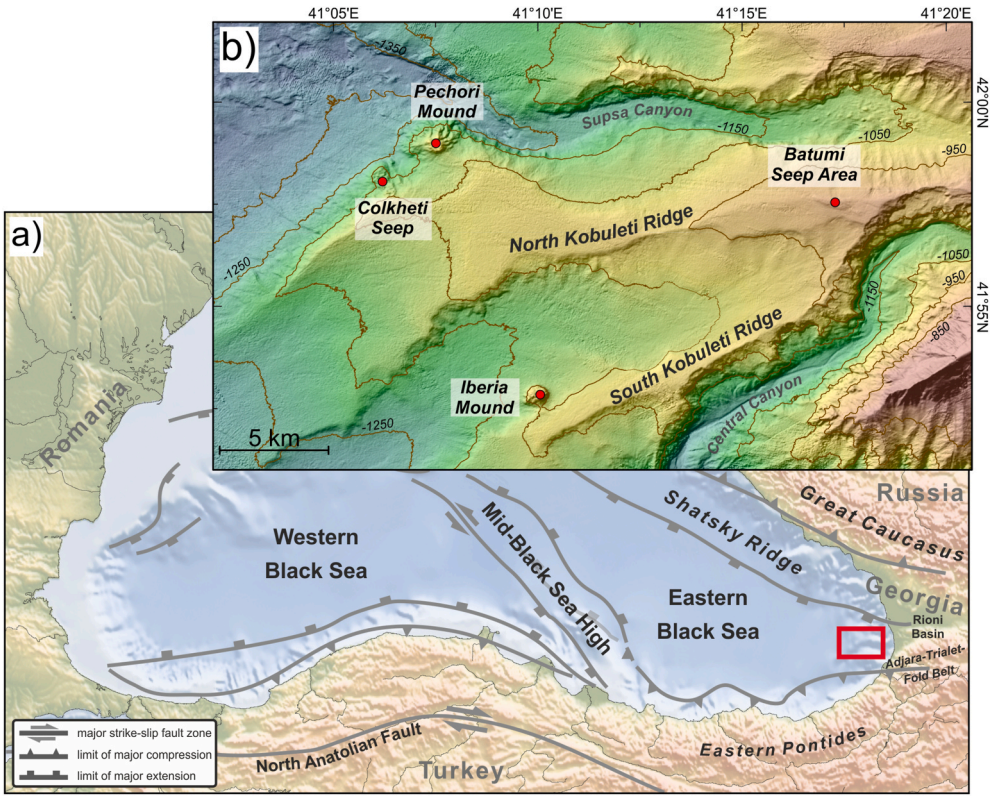

Fig. 1. a: Black Sea bathymetric map showing major tectonic structures (tectonic elements after Robinson et al. (1996) and Starostenko et al. (2004)) and position of the study area (red lined rectangle) in the Gurian thrust-fold belt offshore the southern Rioni foreland basin (Republic of Georgia). **b:** Positions of the studied four gas and oil seep sites associated to the Kobuleti Ridge. Bathymetry contours are in 100-m increments.

severe compressional deformation resulting in the formation of anticlines and development of a series of ~W–E trending canyons and ridges (Klaucke et al., 2006; Nikishin et al., 2015a; Sipahioglu et al., 2013; Tari et al., 2018; Wagner-Friedrichs, 2007).

2.2. Organic matter sedimentology

2.2.1. Pre-holocene sediments

In the region of the South Rioni foreland basin, onshore Georgia, several thick sedimentary units have accumulated since the Paleocene (Tari et al., 2018). With respect to their high organic matter content, post-rift infills belonging to the Middle Eocene (Upper Lutetian – basal Priambonian) Kuma Formation and the Oligocene–Lower Miocene (Rupelian–Burdigalian) Maikop Group are of major interest (Boote et al., 2018; Mayer et al., 2018a, 2018b; Monteloene et al., 2019). Both formations are widespread in the Black Sea and are characterized by a good to very good hydrocarbon formation potential (e.g., Mayer et al., 2018b; Sachsenhofer et al., 2018b). In the Eastern Black Sea area they contain organic-rich units (Kuma – max. 10.3 wt% TOC) (Rupelian part of the Maikop Group – max. 4.8 wt% TOC) (Vincent and Kaye, 2018) and are thermally immature (e.g., Mayer et al., 2018b; and references therein). In the Rioni Basin, the Kuma Formation is composed of fully marine marls and may reach a thickness of about 40 m (Pupp et al., 2018). In contrast, the Rupelian oil-prone part of the Maikop Group contains hemipelagic organic marls and shales and is between 60 and 200 m thick (Pupp et al., 2018; Vincent and Kaye, 2018). The total thickness of the Maikop Group in the South Rioni foreland basin may reach up to 800 m (Pupp et al., 2018; Tari et al., 2018). Post-Rupelian parts of the Maikop Group consist of a series of thin-bedded sandstones and marls overlain by organic shale (Tari et al., 2018).

Boote et al. (2018) and Sachsenhofer et al. (2018a) suggested that the Kuma Formation is tentatively the more significant source of oils in the Eastern Paratethys region if compared to the Maikop Group. At the Shromisubani oil field, onshore Georgia some 50 km distant to the Batumi seep area, biomarker distributions and compound-specific stable carbon isotopic compositions in two oil samples from reservoir rocks were interpreted to represent a hydrocarbon mixture generated from both, the Kuma Formation and the Oligocene part of the Maikop Group (Mayer et al., 2018b).

From Early to Late Miocene, sediments appear to be mostly sandy clastics including sandy marl, sandstones and siltstones (Adamia et al., 2010, 2011; Shillington et al., 2008; Tari et al., 2018). From Late Miocene to Late Pliocene, sand- and claystones, carbonates, siderites, clays, black shales and various conglomerates that can reach a total thickness of more than 1 km occur (Adamia et al., 2010, 2011; Tari et al., 2018). Pleistocene deposits in the Rioni foreland basin comprise sandy clastics including sandy shales, sandy beds, sandstones and gravel beds (Tari et al., 2018).

2.2.2. Holocene sediments

Since the Late Glacial, sediments deposited under limnic to marine conditions accumulated widespread in the Black Sea (Bahr et al., 2006; Ross and Degens, 1974; Soulet et al., 2011). They are usually classified into (at least) three sedimentary units. The lowermost deposits consisting of late Pleistocene-early Holocene (until ca. 8.9 kyrs calBP) lacustrine mud are assigned as Unit III. This is overlain by a mid-Holocene sapropel (Unit II; ca. 7.7–2.8 kyrs calBP). The uppermost Unit I comprises of finely laminated late Holocene coccolith ooze.

At the time of Unit III-II transition the Black Sea turned into a well stratified water body with a permanently anoxic deep-water layer (e.g., Özsoy and Ünlüata, 1997; Soulet et al., 2011). Thus, sapropelic deposits that comprise TOC contents exceeding 10% (Calvert and Karlin, 1998) mainly represent Unit II sediments. Close to the study sites investigated herein, TOC contents maximized at 5.6% in Unit II deposits (Pape et al.,

2010). Currently, organic matter in the Black Sea is mainly supplied by major rivers draining into the western basin (e.g., Danube, Dnepr, Dnestr, Don). Due to permanent anoxia below approximately 80–140 m mbsl (Özsoy and Ünlüata, 1997), the anoxic organic matter decay is less effective particularly in the euxinic water body (Pedersen and Calvert, 1990) resulting in the accumulation of organic-rich modern sediments with TOC contents around 2%. In the study area, Late Glacial and Holocene sedimentation have likely been affected by fluvial input from rivers sourced from the Caucasus (Wagner-Friedrichs, 2007) as well.

2.3. Hydrocarbon seeps in the Eastern Black Sea area

Compressional uplift of anticlines led to the formation of a complex system of SW–NE to W–E trending canyons and ridges at the offshore extension of the Rioni foreland basin (Sipahioglu et al., 2013; Tari et al., 2018; Tari and Simmons, 2018; Wagner-Friedrichs, 2007). In several cases, the uparching of anticlines buried below the ridges appears to have affected formation of near-vertical faults, which along with upward domed lithological boundaries might serve as fluid migration pathways (Tari and Simmons, 2018). At several sites, intense gas and oil expulsion typically occur on top of the ridges or on the flanks of the ridges at water depths between about 830 and 1,140 mbsl (Klaucke et al., 2005, 2006).

Past research focused on four gas and oil seeps (Batumi seep area, 840 mbsl; Iberia Mound, 990 mbsl; Colkheti Seep, 1,120 mbsl; Pechori Mound, 1,020 mbsl) associated to the Kobuleti Ridge (Fig. 1b) (Akhmetzhanov et al., 2007; Bohrmann et al., 2007; Klaucke et al., 2006; Körber et al., 2014; Nikolovska et al., 2008; Pape et al., 2010; Reitz et al., 2011). All these hydrocarbon seeps showed at least episodic gas escape from the seafloor, whereas the latter three are characterized by additional oil impregnations in shallow sediments or even by oil seepage. Based on oil slick dimensions on the sea surface visualized by remote sensing, the Colkheti Seep and the Pechori Mound appear to be the most potent in the Black Sea with respect to emitted oil (Evtushenko and Ivanov, 2013; Körber et al., 2014). However, the burial depth of the respective gas and oil source rocks remained largely unknown, so far.

Gas hydrates diagnostic for methane supersaturation have been found in shallow sediments (>90 cm below seafloor; cmbsf) at all four seep sites (Akhmetzhanov et al., 2007; Bohrmann et al., 2007; Heeschen et al., 2011; Klaucke et al., 2006; Pape et al., 2010, 2011). In addition, sulfate reduction in the upper tens of cm substantiate a very shallow sulfate-methane interface (SMI) and AOM zone supported by intense upward flux of methane (Reitz et al., 2011). The presence of authigenic carbonates at all study sites indicates that hydrocarbon charging of shallow sediments persisted already for a relatively long time (Bahr et al., 2010; Bohrmann et al., 2007).

2.3.1. Study sites

2.3.1.1. Batumi seep area. At Batumi seep area, which is located about 40 km west of the Georgian coast on Kobuleti Ridge at about 840 mbsl (Fig. 1b), almost pure gas emission occurs. The seep area forms a smooth, up to 10 m-high, irregular seafloor elevation covering an area of approx. 0.5 km^2. Gas bubbles escaping the seafloor were found to rise in the water column (Nikolovska et al., 2008), and calculations showed that methane fluxes are in the range of other well-known hydrate-related seep areas (Haeckel et al., 2008). Presence of oil in this area did not become apparent neither in remote sensing data (Körber et al., 2014), nor in recovered near-surface sediments or during ROV-based seafloor inspections. From seismic reflectance, it was inferred that gas ascent and emission is related to vertical faults, which cut through well-defined sediment packages in the GHSZ and have connection to gas accumulations below (Wagner-Friedrichs, 2007). Seafloor backscatter anomalies were interpreted as indications either for gas enrichments, or for the presence of shallow gas hydrates and/or authigenic carbonates, which all were confirmed by groundtruthing (Bahr et al., 2010; Bohrmann et al., 2007; Klaucke et al., 2006; Pape et al., 2010).

2.3.1.2. Iberia Mound. Iberia Mound is located on the southern rise of Kobuleti Ridge at about 990 mbsl (Fig. 1b). It is a cone-shaped structure of about 30 m seafloor elevation and >1 km in diameter (Akhmetzhanov et al., 2007; Körber et al., 2014). Seismic records suggested the presence of a feeder channel similar in diameter to the seafloor expression itself that connects upward bulged reflectors at depth and the shallow subsurface (Wagner-Friedrichs, 2007). The seismic data from the deep subsurface was initially interpreted to illustrate a diapiric structure (Wagner-Friedrichs, 2007) and later associated to a toe-thrust anticline (Tari and Simmons, 2018). The evolution of Iberia Mound was attributed to upward transport of gas-saturated material within the conduit (Wagner-Friedrichs, 2007). Gas flares indicative for gas bubble escape from the seafloor were observed (Akhmetzhanov et al., 2007). Gravity cores contained either the common hemipelagic Black Sea sediments or mud breccia, and oil-staining was observed for sediments below about 60 cmbsf (Akhmetzhanov et al., 2007; Bohrmann et al., 2007). However, in contrast to Colkheti Seep and Pechori Mound, the presence of oil slicks at the sea surface identifiable by remote sensing has not been reported, so far.

2.3.1.3. Colkheti Seep. Colkheti Seep is positioned at the northwestern rise of Kobuleti Ridge at about 1,120 mbsl (Fig. 1b). It forms an asymmetric cone-shaped elevation with a relief of ca. 20 m and a diameter of ca. 1.4 km (Körber et al., 2014). From seismic reflectance, the presence of upward bulged sediments was inferred (Bohrmann et al., 2007; Wagner-Friedrichs, 2007). Moreover, fluid upward migration from toe-thrust anticlines at greater depth fueling oil-impregnations at the sea bed and oil slicks at the sea surface was proposed (Tari and Simmons, 2018). However, the composition of pore waters in shallow sediments did not support a deep origin of upward migrating fluids (Reitz et al., 2011). For shallow sediments, which appeared to be heavily deformed, seismic data revealed the presence of gas and gas hydrate accumulations (Bohrmann et al., 2007). Near-surface sediments comprised the common hemipelagic Black Sea series that was typically oil-stained up to the sediment top (Akhmetzhanov et al., 2007; Körber et al., 2014). Gas hydrates, that occurred at depths exceeding 130 cmbsf, where oil-stained as well. Episodic oil slick occurrence on the sea surface in recent years substantiate considerable oil discharge from the Colkheti Seep (Evtushenko and Ivanov, 2013; Körber et al., 2014).

2.3.1.4. Pechori Mound. Pechori Mound is located at about 1,020 mbsl on the northwestern crest of Kobuleti Ridge (Fig. 1b) and provides gas and oil seepage. It is a cone-shaped structure with a seafloor diameter of about 2.0–2.5 km, and a relief of about 75 m (Körber et al., 2014). Pechori Mound is characterized by weak and chaotic near-seafloor reflection patterns attributed to the presence of shallow gas or gas hydrate accumulations (Bohrmann et al., 2007). A vertical acoustic transparent zone beneath as wide as the mound diameter and connected to buried upward-bulged reflectors was interpreted to represent a pathway for the ascent of gas-saturated, homogenous mud (Akhmetzhanov et al., 2007; Wagner-Friedrichs, 2007). In sediment cores taken close to the center, clasts including mudstones and mud breccia diagnostic for material upward transport were frequently found (Akhmetzhanov et al., 2007; Bohrmann et al., 2007). Gas hydrates present in near-surface deposits indicate considerable fluid from below (Reitz et al., 2011). Similar to the Colkheti Seep, both the sediments and embedded gas hydrates were often found to be stained by oil impregnations, and slicks of natural oil were recognized on the sea surface (Bohrmann et al., 2007; Evtushenko and Ivanov, 2013; Heeschen et al., 2011; Körber et al., 2014). From the chemical composition of pore fluids, Reitz et al. (2011) proposed deep fluid advection as well as fluid alteration by mineral–water reactions at elevated temperatures (60–110 °C) taking place at Pechori Mound.

3. Sampling, sample preparation and analytical procedures

3.1. Sampling and preparation

Samples investigated in this study (Table A1 in Appendix) were obtained during four field campaigns in June 2005 (RV 'Professor Logachev', cruise TTR-15, UNESCO Training Through Research Program), March/April 2007 (RV 'METEOR', M72/3a and b), May 2010 (RV 'MARIA S. MERIAN', MSM15/2), and March 2011 (RV 'METEOR', M84/2). Seafloor inspections using the remotely operated vehicles (ROVs) 'Cherokee' or 'MARUM-QUEST 4000m' were conducted during cruises TTR-15, M72/3a, and MSM15/2 prior to groundtruthing.

3.1.1. Sediments

Pressurized sediment cores up to 2.65 m in length were recovered with the Dynamic Autoclave Piston Corer (DAPC; for description see Abegg et al., 2008; Heeschen et al., 2007; Pape et al., 2010). Non-pressurized sediment cores were recovered with gravity corers (GrC; 3 or 6 m core length), multi and mini corers (MUC and MIC; <0.5 m). The cutting barrel of the GrC was occasionally lined with a tubular plastic foil instead of a PVC-liner conventionally used in order to enable immediate access to gas hydrate pieces. Because lengths of gravity cores have not been corrected for potential loss of uppermost sediments during core recovery, sediment depths are reported as 'core depths'. Additional surface sediments were collected by push coring (PC, <0.30m) conducted with the ROV 'MARUM-QUEST 4000m'.

Sediments were sampled from GrC in 5–40 cm-resolution on deck, subsequently transferred into a cold room (4–8 °C), and prepared under temperatures similar to bottom water temperature (~8.9 °C). MUCs, MICs, and PCs were transferred immediately upon recovery into the cold room and sampled in 0.5–3 cm resolution.

3.1.2. Oil

Oil-water mixtures present in sediment cores were sampled during cruise MSM15/2 at Colkheti Seep from a depressurized DAPC core (GeoB14345). Oil slicks floating on the sea surface above Colkheti Seep were collected within 48 h upon pressure coring in 1L-glass bottles (screw cap with Teflon inlet). The glass bottles were manually filled from a dinghy, and the samples were diluted with sodium azide (0.02%; w/v) to inhibit microbial attack. During time of sampling, gas-oil bubbles that disintegrated while reaching the sea-atmosphere boundary and left oil slicks on the sea surface were observed.

3.1.3. Sedimentary gas, hydrate-bound gas and free gas

Sediment cores were taken under in situ hydrostatic pressure with the DAPC (Abegg et al., 2008) for the determination of in situ gas concentrations, molecular compositions (C_1 to C_5-hydrocarbons, CO_2), and stable C and H isotopic compositions (C_1, C_2, and C_3). The recovered gas was released from the DAPC pressure chamber via a 'gas manifold' (Heeschen et al., 2007; Shipboard Scientific Party, 1996), and gas sub-samples were transferred into glass serum vials prefilled with NaCl solution for later analysis as reported elsewhere (Pape et al., 2010). For vertical profiling of C_1 to C_3 hydrocarbon concentrations and stable C isotopic compositions of methane, gases were stripped from the sediments (taken by GrCs, MUCs, MICs, and PCs). For this, 3 mL of bulk sediment were transferred immediately after recovery into 20 mL crimp-top vials pre-filled with 5 mL 1 M NaOH (see Reitz et al., 2011). Gas hydrate samples were extracted from gravity cores or from longer sediment cores recovered with the seafloor drill rig MARUM-MeBo70 (Bohrmann et al., 2011) from all seeps sites investigated for analysis of the molecular composition and stable C and H isotopic ratios of hydrate-bound volatiles. The hydrate pieces were extracted from the cores immediately upon recovery, cleaned with ice-cooled purified water, filled into gas-tight syringes, and left for dissociation at ambient temperature. The released gas was transferred into glass serum vials as described above. Gas escaping the seafloor at Colkheti Seep and the Batumi seep area was collected several centimeters above the seabed with the Gas Bubble Sampler (GBS) operated by an ROV (Pape et al., 2010; Sahling et al., 2009). The gas was released from the GBS pressure chamber via the gas manifold and injected into glass serum vials for storage as described above.

3.2. Analyses

An overview of the different analytical methods applied to the multiple types of samples investigated in this study is given in Table A2 in Appendix.

3.2.1. Analysis of sediments – organic extracts, fractions, and individual compounds

For analysis of mid-to high-molecular weight hydrocarbons (ca. C_{15} to C_{35}), organic compounds were extracted from sediment samples with dichloromethane (DCM) using an accelerated solvent extractor (Dionex ASE-200), and from the water samples by use of a separatory funnel. For ASE, 10 g of the sediment sample was diluted with 22 g sea sand (extracted and annealed, 4 h at 400 °C) within extraction cells. Organic extracts were collected automatically, and elemental sulfur was subsequently removed from the extract by treatment with activated (10% HCl at 60 °C for approximately 1 h) copper granula. Two oil-water mixtures from the sea surface above the Colkheti Seep were extracted with DCM using ultrasonification.

Asphaltenes contained in the extracts were precipitated by adding 2 mL DCM and 60 mL petroleum ether to 100 mg of extract in maximum. After 12 h reaction time, the extracts were centrifuged at 3,000 rpm for 15 min. The supernatant solution containing maltenes and resins was collected and the solvent removed through evaporation in a N_2-atmosphere at 35 °C. For samples that yielded more than 10 mg of extract, the residual maltenes and resins were separated into aliphatic and aromatic fractions as well as into hetero-compounds (NSO-compounds) on silica gel (activated at 240 °C for 12 h) by mid-pressure liquid chromatography using a sequence of organic solvents of increasing polarity (*i*-hexane, *i*-hexane/DCM (2:1; v:v), DCM/methanol (2:1; v:v)). For samples with extract amounts below 10 mg, only the aliphatic fraction was retrieved from the chromatographic column.

Compound distributions in the aliphatic fraction were determined with an Agilent 6890 gas chromatograph (GC) equipped with a 50 m Ultra 2 column (Agilent; 0.2 mm inner diameter; 0.11 μm film thickness) and connected to a flame ionization detector (FID). Individual aliphatic biomarkers were analyzed by GC separation and subsequent mass spectrometric determination by a coupled GC (Agilent 6890) mass spectrometer (MS; Finnigan MAT95S) system. Measurements were carried out as multiple-reaction-monitoring using parent-daughter-scans.

For analysis of stable carbon isotope ratios ($\delta^{13}C$) of the saturated and aromatic hydrocarbon fractions as well as the NSO fraction, they were placed in Ag-melting pots (with minimum 100 μg C). $\delta^{13}C$ values were determined with a coupled Carlo Erba NC 2500 elemental analyzer (EA) and a Thermo Scientific DeltaPlus isotope ratio mass spectrometer (IRMS). The reproducibility of $\delta^{13}C$ analyses was ±0.2‰. Carbon isotope values given herein are reported in the δ-notation vs. the Vienna Pee Dee Belemnite (V-PDB) standard, respectively.

3.2.2. Analysis of volatiles

Concentrations of C_1 to C_3 hydrocarbons extracted from gravity cores GeoB11970 and 11971 (Colkheti Seep) were analyzed using a GC (Carlo Erba, GC 8000 top; Reitz et al., 2011). Replicate measurements of standard hydrocarbon mixtures showed a precision of 1–3 mol-%. Additionally, molecular distributions of C_1 to C_5 hydrocarbons and CO_2 in sedimentary gas from pressurized cores, in vent gas collected with the GBS, and in hydrate-bound gas collected at Iberia Mound, Colkheti Seep and Pechori Mound were analyzed with a two-channel GC (Pape et al., 2010) either on board or in the home lab within six weeks after sampling. Calibrations and performance checks of the analytical system

were conducted using commercial pure gas standards and gas mixtures (Air Liquide, Germany). The coefficient of variation determined for the analytical procedure was <2%.

Stable C isotope ratios of methane extracted from non-pressurized sediment cores (GrC, MUC, MIC, PC) were analyzed by GC-combustion-isotope ratio monitoring mass spectrometry (GC-C-IRMS; see Reitz et al., 2011). Stable C isotope ratios of C_1 to C_3 hydrocarbons and CO_2 in sedimentary gas from pressurized cores (DAPC), vent gas, and hydrate-bound gas were analyzed by GC-C-IRMS as reported elsewhere (Pape et al., 2010). Stable H isotope ratios (δ^2H) of methane prepared from the various gas types were analyzed at the GCA–Geochemische Analysen commercial laboratory (Sehnde-Ilten, Germany) by GC separation (Hewlett-Packard 5840 II) of methane from other light hydrocarbons followed by on-line pyrolysis (carbon

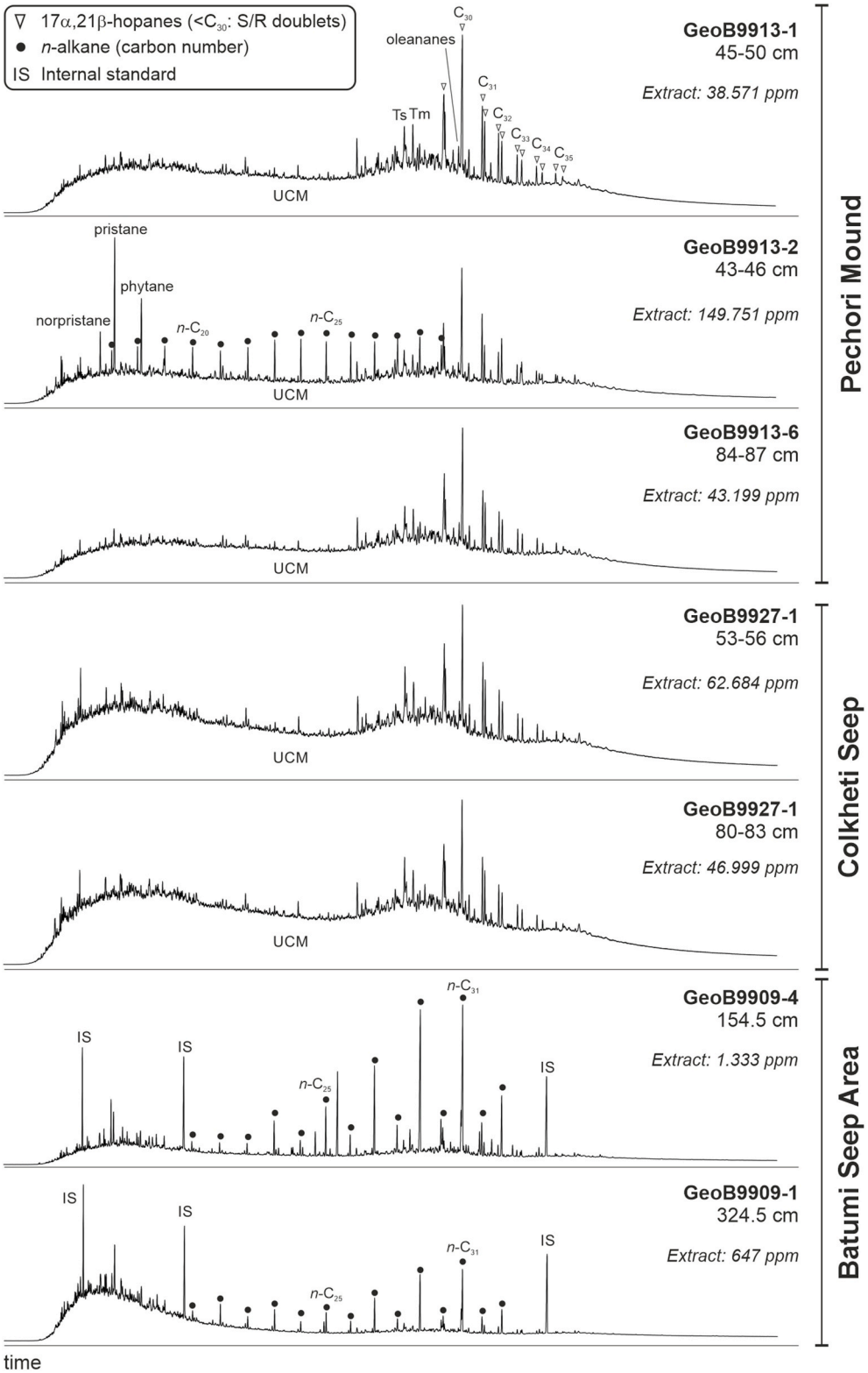

Fig. 2. Gas chromatograms of aliphatic hydrocarbons extracted from sediments of the Pechori Mound, the Colkheti Seep, and the Batumi seep area indicating strong impregnations with oil-stemming compounds (e.g., *n*-alkanes without odd-even predominance, pristane and phytane, and hopanes) for Pechori Mound and Colkheti Seep. The high abundance of hopanes and unresolvable complex mixtures (UCM) shows a generally high degree of biodegradation. The number after "Extract" gives the amount of extractable organic matter in the respective sediments (calculated on dry weight sediment; adopted from Reitz et al., 2011). Depth indications in centimeter core depth.
At the Batumi seep area oil-derived hydrocarbons are also present although in much lower concentrations and are overlain by allochthonous sub-recent organic matter (here higher *n*-alkanes from terrestrial plants). Oleananes include the 18α- and 18β (H)-isomer. Note: Sediments from Iberia Mound have not been analyzed.

microfilm in Al_2O_3 tube, 1195 °C) according to Tobias and Brenna (1997). Hydrogen was separated from other gases in a 0.5 m packed column (M5A, 1/16″), and stable H isotope ratios were measured online in a EUROPA 20-20 continuous flow IRMS.

4. Results and discussion

Sediment and gas samples from four gas and oil seepage sites in the Eastern Black Sea were investigated in order to gain information about the depositional environment, the burial depth, the degree of maturity of organic matter sourcing hydrocarbons present in shallow deposits, and potential chemical alterations during migration. Parts of the organic matter and fluids data at the four hydrocarbon seeps have been reported in Pape et al. (2010) and Reitz et al. (2011).

4.1. Sources of organic matter and light hydrocarbons

4.1.1. General characterization, origin and depositional regime of organic matter present at the seep sites

In order to characterize the origin of the organic matter sourcing hydrocarbons in surface sediments, diagnostic aliphatic biomarkers in sediments from the four hydrocarbon seeps were investigated in this study. In a previous study, these sediments were analyzed for abundances and compositions of bulk organic fractions. For instance, large amounts of extractable organic matter spanning from 650 ppm (Batumi seep area) to 150,000 ppm (Pechori Mound) of sediment weight showed that particularly Colkheti seep and Pechori Mound sediments were heavily impregnated by oil (Reitz et al., 2011). In addition, compositions of maltenes and resins in sediments from Colkheti Seep and Pechori Mound were found to be diagnostic for typical crude oils supporting the relevance of oil injections at these sites (Fig. 2).

Distribution patterns of aliphatic hydrocarbons analyzed in this study were characterized by unresolvable complex mixtures (UCM) represented by humps in different degrees in the chromatograms that indicate substantial degradation of organic matter (Fig. 2). Individual biomarkers were mainly comprised of linear alkanes, acyclic isoprenoids, and tetra- and pentacyclic isoprenoids (steranes and hopanes) with carbon numbers ranging from about 16 to 35 carbon atoms. For samples from the Batumi seep area an odd-over-even prevalence of linear components, attributable to an origin from leaf waxes of higher plants (Eglinton et al., 1962) was found. Relative abundances of C_{27}- to C_{29}-sterane isomers (ca. 20/38/42 mol-% of all C_{27}–C_{29}-sterane isomers) indicate that organic matter comprises of a mixture of land plants and marine planktonic organic matter (Fig. 3a).

Isomers of the pentacyclic triterpenoid oleanane (and degradation products like de-A-oleanane) were present in sediments of all sites investigated (and also in the oil-water mixtures taken at the sea surface above Colkheti Seep). The occurrence of oleanane, which results from certain angiosperms plants (Ekweozor et al., 1979), at the Batumi seep area, the Colkheti Seep and the Pechori Mound along with the relatively high oleanane-index (12–19; see also Reitz et al., 2011) hints to a near-shore origin of the source rock (Table 1, Fig. 3b). This interpretation is corroborated by the ratio of C_{31}-22*R*-versus C_{30}-hopanoids (mostly around 0.25), which is potentially indicative for a mixed source rock facies of lacustrine and marine origin (Peters et al., 2004).

4.1.2. Age and maturity of organic matter

Indications for the age of the source rock(s) were gained from the presence of source-diagnostic hydrocarbons and stable carbon isotopic signatures of bulk hydrocarbon fractions. The presence of the angiosperm-biomarker oleanane (Fig. 3b; see also Reitz et al., 2011) suggests that the deposition of the source rock took place during the Upper Cretaceous or later times (Moldowan et al., 1994; Riva et al., 1988).

Further indications for the sourcing rock and, thus, indirectly for its age were deduced from the stable carbon isotopic signatures of the saturated and aromatic hydrocarbon fractions. Stable carbon isotopic signatures of the aliphatic hydrocarbon fraction were −26.5‰ and −26.6‰ for Colkheti Seep and −27.1‰ to −27.3‰ for Pechori Mound, while $\delta^{13}C$ values of the aromatic hydrocarbon fraction were −25.6‰ and −25.8‰ at Colkheti Seep and −26.2‰ to −26.4‰ at Pechori Mound (Table 1, Fig. 4). These values suggest i) that aquatic organic matter is the prevalent hydrocarbon source at the study sites (Sofer, 1984) and ii) that the petroleum at the different sites originates from same source rocks. These data further point at deposits younger than Late Cretaceous in age and in particular at those of the Eocene Kuma Formation and the Oligocene–Lower Miocene Maikop Group, since both are rich in organic matter and have significant hydrocarbon potentials

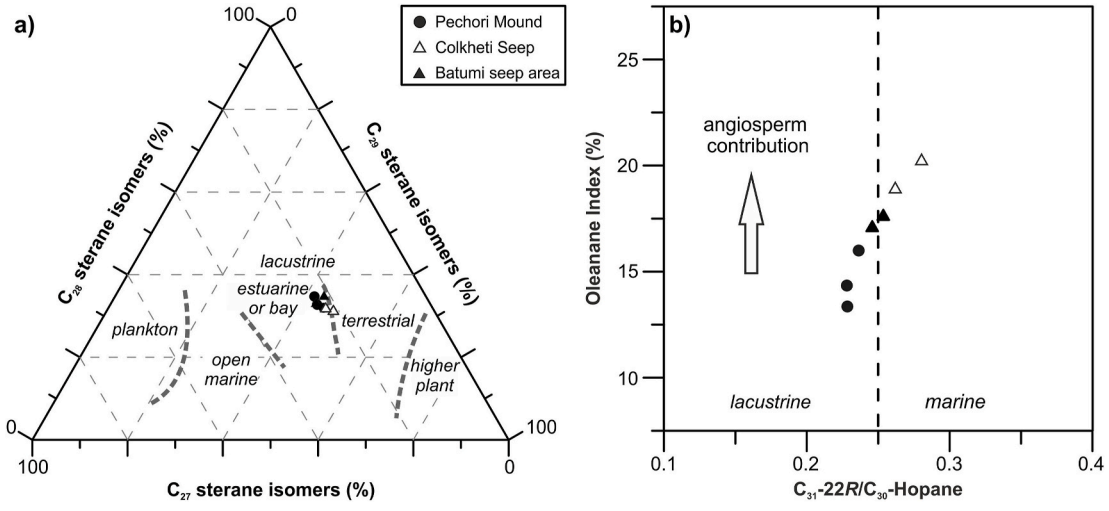

Fig. 3. a: Relative proportions of C_{27}- to C_{29}-sterane isomers indicate that organic matter from the Batumi seep area, Colkheti Seep and Pechori Mound is primarily characterized by contributions from land plants and planktonic organisms. Classification according to Huang and Meinschein (1979). For sample codes see Table 1. **3b:** C_{31}-22*R*/C_{30}-hopane ratio vs. the oleanane index (Oleanane/(Oleanane + C_{30}-hopane) x 100). The C_{31}-22*R*-/C_{30}-hopane ratio is commonly used to distinguish between lacustrine and marine depositional environments (threshold 0.25; Peters et al., 2004). C_{31}-22*R*-/C_{30}-hopane ratios for the samples studied herein do not allow for an unambiguous assignment of lacustrine or marine depositional conditions. However, the presence of the biomarker oleanane in high abundance, as expressed by relatively high values of the oleanane index (>12%), indicates a significant contribution from angiosperm remnants to the organic matter. For sample codes and values see Table 1. Note: Values of sea surface oil slick samples from Colkheti Seep are outside of the area shown.

Table 1
Biomarker ratios indicative for the maturity of the source rock, together suggesting similar maturities for all samples (early oil to early peak oil). Hop = 17α,21β(H)-hopane; Mor = 17β,21α(H)-hopane; Ts = 22,29,30-trisnor-18α-neohopane; Tm = 22,29,30-trisnor-17α-neohopane.

Core depth (cm)	Sample code (GeoB)	20S/(20S+20R) αα-C_{29}-sterane[c]	ββ/(αα+ββ)-C_{29}-sterane[d]	22S/(22S+22R)-C_{32}-αβ-hopane[e]	Hop/(Mor+Hop)[b,f]	Ts/(Ts+Tm)[b,g]	O/(O+C_{30}-Hop)x100	22R–C_{31}/C_{30}-hopane)	$\delta^{13}C$ aliphatic fraction	$\delta^{13}C$ aromatic fraction
Pechori Mound										
(45–50)	9913–1	0.51	0.52	0.59	0.92	0.57	13.3	0.23	−27.2	−26.4
(43–46)	9913–2	0.48	0.49	0.59	0.92	0.56	14.3	0.23	−27.3	−26.2
(84–87)	9913–6	0.55	0.50	0.58	0.92	0.57	15.9	0.24	−27.1	−26.2
Colkheti Seep										
(53–56)	9927–1	0.47	0.51	0.58	0.90	0.67	20.3	0.28	−26.6	−25.8
(80–83)	9927–1	0.44	0.41	0.59	0.90	0.67	19.0	0.26	−26.5	−25.6
Sea surface slick (# 2)		0.49	0.52	0.58	0.86	0.64	29.8	0.47	na	na
Sea surface slick (# 3)		0.48	0.51	0.58	0.90	0.67	22.7	0.29	na	na
Batumi seep area										
(154.5)[a]	9909–4	0.41	0.45	0.58	0.89	0.60	17.1	0.25	na	na
(324.5)[a]	9909–1	0.38	0.45	0.58	0.90	0.64	17.6	0.25	na	na

na = not analyzed.
[a] Note that ratios most likely reflect a mixture of lowly concentrated oil and immature sub-recent organic matter.
[b] also related to source.
[c] Equilibrium = 0.52–0.55 at %R_o 0.8 (Killops and Killops, 2013; Seifert and Moldowan, 1986).
[d] Equilibrium = 0.67–0.71 at %R_o 0.9 (Seifert and Moldowan, 1986).
[e] Equilibrium = 0.57–0.62 at %R_o 0.6 (Seifert and Moldowan, 1980).
[f] Equilibrium = 0.95 at %R_o 0.7 (Killops and Killops, 2013).
[g] Equilibrium = 1 at %R_o 1.3 (Killops and Killops, 2013).

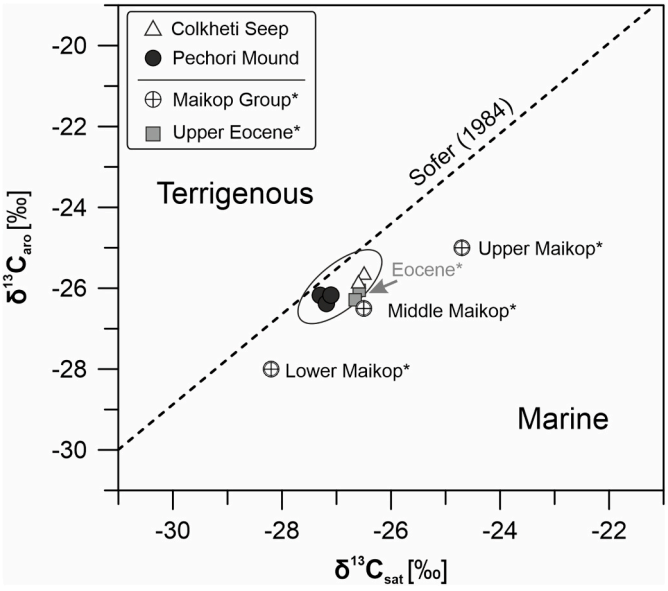

Fig. 4. Cross-plot (after Sofer (1984)) indicating bulk stable carbon isotopic values of aromatic hydrocarbons ($\delta^{13}C_{aro}$) and saturated hydrocarbons ($\delta^{13}C_{sat}$) in organic extracts from samples collected at the Colkheti Seep and the Pechori Mound. *Values determined for petroleum belonging to the Lower to Upper Maikop Group (Abrams and Narimanov, 1997) and for Upper Eocene sediments (Bechtel et al., 2014) from the western South Caspian Depression are shown for comparison. For sample codes and values see Table 1.

(e.g., Boote et al., 2018; Pupp et al., 2018; Sachsenhofer et al., 2018a; 2018b; Vincent and Kaye, 2018). In the Rioni basin, oil-prone type II kerogen is dominant in the Kuma Formation, whereas deposits of the Maikop Group are characterized by oil to gas-prone type II–III and type III kerogen (Pupp et al., 2018).

Several geochemical parameters including hydrocarbon isomerization ratios were used to evaluate the thermal maturity of the source rock at the study sites (Table 1). At all sites hydrocarbon biomarker isomers are in line with early oil-window maturity of the source rock. Although not considerably lower than samples from the other seep sites, samples from the Batumi seep area represent the lowest calculated vitrinite reflectance equivalents (in R_o% = % reflectance in oil) as exemplified by

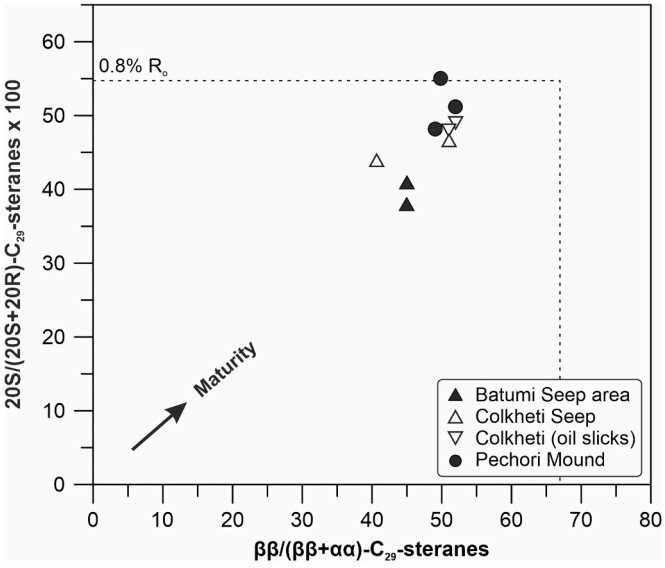

Fig. 5. Relative abundance of sterane isomers at the studied sites and inferred tentative maturity in vitrinite reflectance in oil (R_o; Killops and Killops, 2013). Increasing numbers (until equilibrium of isomerization; see Table 1) denote increasing maturity (Batumi seep area < Colkheti Seep/Pechori mound). All samples (including Colkheti Seep oil slicks) are in line with early oil window maturity. For sample codes and values see Table 1 and Table A1 in Appendix.

20S(20S+20R)αα-C_{29}-sterane and ββ/(αα+ββ)-C_{29}-sterane ratios (Fig. 5).

4.1.3. Isotopic and molecular compositions of volatiles ascending at the seep sites

At the Batumi seep area highest relative abundances of methane (99.94 mol%) amended by traces of non-methane hydrocarbons (C_2–C_5) and CO_2 resulting in C_1/C_{2+} ratios of 2,498–4,169 were present in vent gas, hydrate-bound gas and in gas from pressure cores (Table 2; Pape et al., 2010; Reitz et al., 2011). Even though gas samples from the oil seeps were characterized by much higher concentrations of non-methane light hydrocarbons, they were also dominated by methane. Relationships between C_1/C_{2+} ratios and $\delta^{13}C$–CH_4 (Fig. 6a) suggest that light hydrocarbons at the four seep sites mainly originate from a mixture of oil-associated thermogenic and secondary microbial hydrocarbons. Whereas oil-associated thermogenic gas is part of the biodegradation feedstock (Milkov and Etiope, 2018), secondary microbial hydrocarbons are formed from biodegradation of other light hydrocarbons, liquid alkanes, and other organic compounds (Head et al., 2003; Etiope et al., 2009; Milkov, 2011). Methane is the predominant secondary microbial hydrocarbon formed. While most of the gas samples from the four seep sites plot in the range that is representative for secondary microbial hydrocarbons, some samples from Colkheti Seep and Pechori Mound plot closer to the field assigned for oil-associated thermogenic hydrocarbons. This interpretation is in accordance with comparably high abundances of C_2–C_5-hydrocarbons (C_1/C_{2+} = 10–1,560) and of CO_2, which are commonly attributed to thermal cracking of organic matter (e.g., Abrams et al., 2009; Bernard et al., 1976, 1977; Schoell 1983, 1988). It also goes in line with the presence of deeply-rooting feeder channels inferred from reflection seismics at Iberia Mound and Pechori Mound (Wagner-Friedrichs, 2007), and fractures proposed at Colkheti Seep and Iberia Mound (Tari and Simmons, 2018). Such subsurface structures may facilitate upward migration of oil-associated hydrocarbons generated from a deeply-buried, relatively low mature source rock. Highest C_1/C_{2+} ratios determined for samples from the Batumi seep area relative to those of samples from the oil seep sites (Fig. 6b) are attributable to a larger fraction of secondary microbial methane that is typically relatively depleted in ^{13}C and ^{2}H (Fig. 6b). On the other hand, an inferred larger proportion of oil-associated thermogenic hydrocarbons in particular at Pechori Mound and Colkheti Seep would correspond to the higher degree of oil-staining observed for shallow sediments at these sites.

4.1.4. Burial depth of oil and gas source rocks

The most likely sources of oil impregnations and volatiles in surface sediments of the gas and oil seeps investigated here, the Eocene Kuma Formation and the Oligocene-Miocene Maikop Group, are probably buried by more than 1 km of sediment (see e.g., Robinson et al., 1996; Tari et al., 2018). However, the thickness of the sediment cover can be highly variable due to tectonic deformation and uplift (Nikishin et al., 2003, 2015a; Tari et al., 2018; Tari and Simmons, 2018). Formation depths of less than 2.7 km below seafloor (kmbsf) for microbial methane as well as minimum formation depths of ca. 3.0 kmbsf for thermogenic hydrocarbons were proposed for the Batumi seep area previously (Pape et al., 2010). For fluids expelled at Pechori Mound, the minimum formation depth was estimated at 1.2–2.2 kmbsf (Reitz et al., 2011).

In this study, we provide additional organic geochemical data that allow for more integral depth estimates. It should be stressed, however, that formation depths and depth ranges stated below are calculated on basis of linearly extrapolated geothermal gradients only and are considered as maximum depths, since gas and oil formation are primarily controlled by time in addition to temperature.

Table 2
Molecular compositions of hydrocarbons and carbon dioxide (in mol-%Σ[C_1–C_5, CO_2]) in gas samples retrieved by degassing of pressure cores (DAPC), by dissociation of gas hydrates (GrC), and by collection with the Gas Bubble Sampler (GBS) from gas and oil seeps in the Eastern Black Sea. $C_1/C_{2+} = C_1/(C_2$–$C_5)$.

	Sample code	CH_4	C_2H_6	C_3H_8	*i*-C_4H_{10}	*n*-C_4H_{10}	unident. C_5H_{12}	unident. C_5H_{12}	C_1/C_{2+}	CO_2	Remarks	Study
	[GeoB]	[mol-%]	[mol-%]	[mol-%]	[mol-%]	[mol-%]	[mol-%]	[mol-%]		[mol-%]		
Batumi seep area												
Vent gas		99.901	0.019	0.004	0.001				4,163	0.075	(mean, n=5)	*adopted from Pape et al. (2010)*
Hydrate-bound gas		99.940	0.030	0.001					3,224	0.029	(mean, n=7, variable depth),	*adopted from Pape et al. (2010)*
	15236–1	99.426	0.027	0.001			0.001		3,428	0.545		*this study*
	15249–1	99.650	0.039	0.001			0.001		2,430	0.309		*this study*
	15251–1	99.675	0.033	0.001			0.001		2,848	0.290		*this study*
	15260–1	99.595	0.027	0.001					3,557	0.377		*this study*
	15236–2	99.642	0.030	0.001			0.001		3,136	0.325		*this study*
Sedimentary gas (pressure core)		99.930	0.039	0.001					2,498	0.030	(mean, n=9)	*adopted from Pape et al. (2010)*
Iberia Mound												
Hydrate-bound gas	11938	99.867	0.029	0.018	0.016	0.001			1,560	0.069	[a])	*this study*
Colkheti Seep												
Vent gas	11902–1	92.460	0.080	0.307	0.053	0.009	0.002	0.037	189	7.052		*this study*
Hydrate-bound gas	11923	96.165	0.019	0.034	0.002	0.009	0.001	0.037	943	3.733	[a])	*this study*
Sedimentary gas (pressure core)	11922	98.620	0.543	0.082	0.060	0.001	0.002	0.007	142	0.685	[a])	*this study*
	14345	99.062	0.141	0.118	0.139	0.003			247	0.536	[a])	*this study*
Pechori Mound												
Hydrate-bound gas	11955	90.548	0.128	0.109	0.024	0.030			311	9.161	[a])	*this study*
	15255	89.484	0.087	0.029	0.014		0.001		683	10.385	[a])	*this study*
	15256	87.504	0.428	0.048	0.009				180	12.011	[a])	*this study*
	15227–1	85.358	0.260	0.067	0.013	0.021	0.000	0.004	234	14.277	[a]), (mean, n=4)	*this study*
	15227–3	82.019	0.313	5.370	2.496	0.083	0.008	0.005	10	9.705	[a]), (mean, n=11, variable depth)	*this study*

[a] Potentially mixed with abundant oil-associated volatiles (e.g., C_{3+}, CO_2) caused by oil impregnations. For sample codes and position see Table A1 in Appendix.

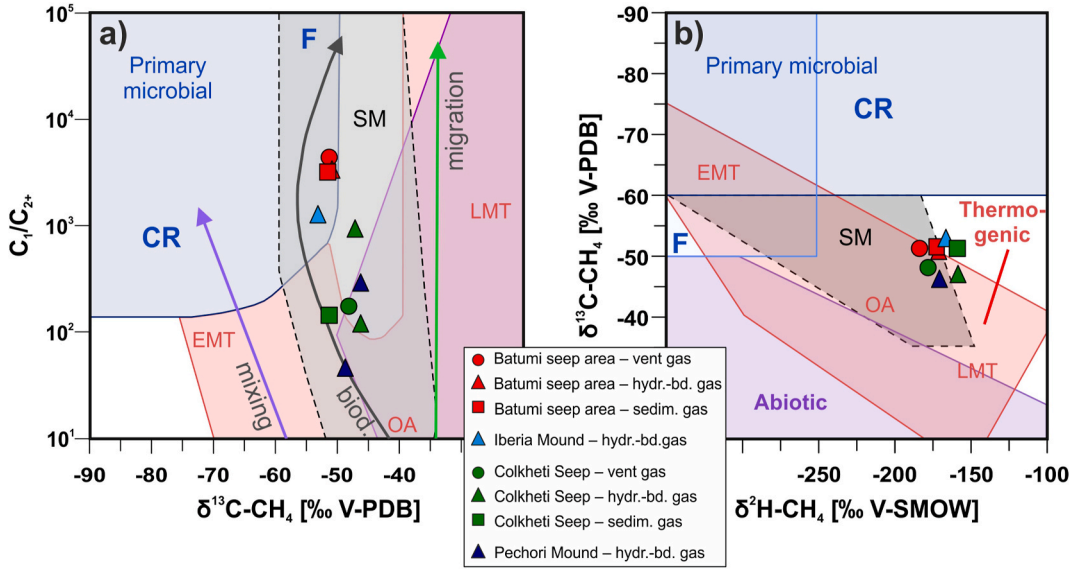

Fig. 6. Generic classifications of light hydrocarbons (adopted from Milkov and Etiope, 2018) in the different gas types (hydr.-bd. = hydrate-bound; sedim. = sedimentary) collected from each of the study sites. CR – carbonate reduction, F – methyl-type fermentation, SM – secondary microbial, OA – oil-associated thermogenic gas, EMT – early mature thermogenic gas, LMT – late mature thermogenic gas. **6a:** C_1/C_{2+} ratios vs. $\delta^{13}C$–CH_4 (modified 'Bernard diagram' after Bernard et al., 1977). Light hydrocarbons from all study sites plot in the fields assigned for oil-associated thermogenic gas ('OA') and secondary microbial gas ('SM') in between the fields representative for early mature and late mature thermogenic gas. Arrows in different colors indicate processes that affect the composition of light hydrocarbons and stable carbon isotopic composition of methane (biod. – biodegradation). Variable degrees of petroleum degradation resulting in different fractions of secondary microbial gas are likely the main causes of the geochemical differences observed for the gas samples from the different study sites. **6b:** $\delta^{13}C$ values vs. $\delta^{2}H$ values of methane in selected gas samples. The results suggest oil-associated thermogenic and secondary microbial production as the major hydrocarbon sources below the four seep sites investigated. For sample codes and values see Table 2 and Table 3. Note: Data for gases from Batumi seep area taken from Pape et al. (2010).

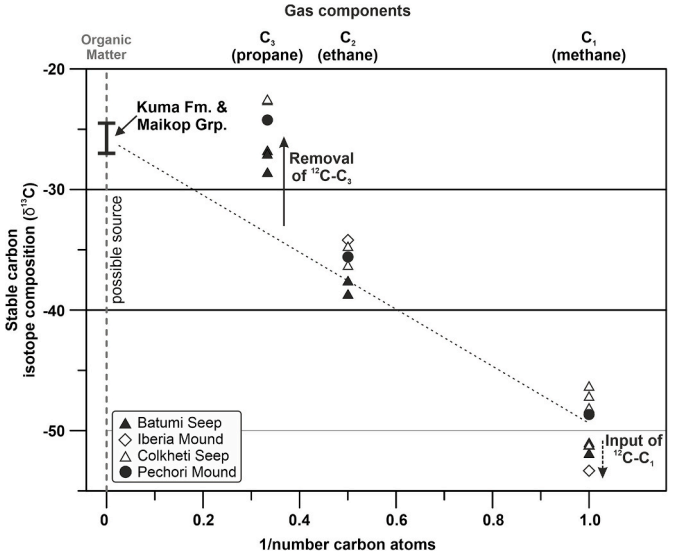

Fig. 7. 'Natural gas plot' (Chung et al., 1988) illustrating $\delta^{13}C$ values of light hydrocarbons versus the reciprocal values of the number of carbon atoms of the respective light hydrocarbon. $\delta^{13}C$-C_{org} of Kuma Formation and Maikop Group (both −27.0‰ to −24.5‰) according to Pupp et al. (2018). $\delta^{13}C$ values of kerogen in rock samples from the Rupelian Maikop Group (−25.3‰ to −25.1‰) and an Kuma suite age equivalent (Late Bartonian–earliest Priabonian; −26.6‰) in NW Georgia have been reported (Vincent and Kaye, 2018; data not illustrated in Fig. 7). Deviations from the line connecting hydrocarbons towards more positive $\delta^{13}C$ values point either to post-genetic consumption or to admixture with component enriched in ^{13}C. In contrast, negative excursions are diagnostic for admixture by ^{12}C-enriched component, e.g., by de-novo-synthesis. Note: Gas samples considered in this diagram comprise sedimentary gas from pressure cores (DAPC), vent gas (GBS), and hydrate-bound gas (GrC); depth resolutions remained unconsidered. For values see Table 3.

Distribution patterns of diagnostic extractable hydrocarbons (Table 1, Fig. 5), stable carbon isotopic compositions of C_2 and C_3 (Table 3, Fig. 7), as well as maturity calculations based on $\delta^{13}C$–CH_4 – $\delta^{13}C$–C_2H_6-relations (e.g., Faber et al., 2015) suggest source rock maturity corresponding to early oil to early peak oil. Temperatures leading to major oil production are typically lower than those that cause substantial light hydrocarbon thermogenesis (70–250 °C with a peak at about 150 °C (e.g., Hunt, 1996; Quigley and Mackenzie, 1988; Seewald, 2003). Considering temperatures typically assumed for early oil production (60–100 °C; e.g., Seewald, 2003) and a linear geothermal gradient of about 26 °C km^{-1} as proposed for the region about 20 km to the south of our study area (Minshull and Keddie, 2010), oil production at the studied sites should principally have taken place at depths between 2.3 kmbsf (60 °C) and 3.8 kmbsf (100 °C). Therefore, the formation depth range of oil-associated thermogenic hydrocarbons calculated in this study is deeper than the minimum source depths (1.2–2.2 kmbsf) that were estimated for fluids expelled at Pechori Mound earlier (Reitz et al., 2011). Unresolvable complex mixtures (UCM) (Figure 2) present in the aliphatic hydrocarbon fractions from all study sites indicate that hydrocarbon degradation occurred, which is thought to be limited to temperatures <80 °C (Wilhelms et al., 2001). Consequently, oil degradation and, thus, secondary microbial methane generation is restricted to depths shallower than 3.1 kmbsf.

4.2. *Post-genetic modifications of hydrocarbons*

4.2.1. *High-molecular weight hydrocarbons*

4.2.1.1. Alterations of high-molecular weight hydrocarbons in sediments. The presence of UCMs in the fractions of aliphatic hydrocarbons (Fig. 2) demonstrates that degradation of higher hydrocarbon took place at all sites investigated. However, the presence of isomers of individual hydrocarbon biomarkers, such as some steranes and hopanes, indicates that biodegradation is not complete. Acylic isoprenoids in samples from the Batumi seep area and the shallowest samples from Pechori Mound

Table 3
Stable isotopic signatures of light hydrocarbons ($\delta^{13}C$ in ‰ V-PDB; $\delta^{2}H$ in ‰ V-SMOW) in vent gas, hydrate-bound gas and pressurized sedimentary gas from gas and oil seeps in the Eastern Black Sea.

Site	Sample code	Sample type	$\delta^{2}H$–CH_4	$\delta^{13}C$–CH_4	$\delta^{13}C$–C_2H_6	$\delta^{13}C$–C_3H_8	Remarks	Study
	[GeoB]		[‰ V-SMOW]	[‰ V-PDB]	[‰ V-PDB]	[‰ V-PDB]		
Batumi seep area		Vent gas	−184	−51.2	−38.7	−28.6	[a]), (n=5)	*adopted from Pape et al. (2010)*
		Hydrate-bound gas	−171	−50.9	−37.6	−27.1	[a]), (n=6)	*adopted from Pape et al. (2010)*
		Sedimentary gas (pressure core)	−172	−51.5	−38.5	−26.8	[a]), (n=5)	*adopted from Pape et al. (2010)*
Iberia Mound	11938	Hydrate-bound gas	−167	−51.9	−34.2			*this study*
Colkheti Seep	11902–1	Vent gas	−180	−47.4	−36.9	−22.5		*this study*
	9931–1	Hydrate-bound gas		−47.0				*this study*
	11923	Hydrate-bound gas	−192	−47.1	−36.3	−22.5		*this study*
	11924	Hydrate-bound gas		−46.3				*this study*
	11971	Hydrate-bound gas	−182	−49.5				*this study*
	11922	Sedimentary gas (pressure core)	−159	−51.2	−36.3	−22.6		*this study*
	14345	Sedimentary gas (pressure core)		−50.4				*this study*
Pechori Mound	11953	Hydrate-bound gas	−210	−47.7	−36.9			*this study*
	11955	Hydrate-bound gas	−171	−47.7	−35.8			*this study*
	15227–3	Sedimentary gas (non-pressurized core)		−50.0				*this study*

[a] = average values calculated from results given for multiple samples in Pape et al. (2010). For sample codes and positions see Table A1 in Appendix.

were dominated by pristane (C_{19}; 2,6,10,14-tetramethylpentadecane) and phytane (C_{20}; 2,6,10,14-tetramethylhexadecane; Fig. 3). Except for the almost oil-free samples from the Batumi seep area in which *n*-alkanes have a mostly sub-recent leaf-wax origin, *n*-alkanes were commonly absent. This clearly demonstrates that the seeping oil was affected by biodegradation to a large extent. However, at station GeoB9913-2 at the northwestern central part of Pechori Mound, *n*-alkanes (along with pristane and phytane) were present, which is indicative for a lower degree of biodegradation. Remarkably, a relation between the intensity of compound-specific degradation and the distances of sampling positions from gas/oil emission sites did not become apparent.

We additionally investigated the potential effects of degradation for oil-gas bubbles during their rise through the water column above Colkheti Seep and Pechori Mound. Oil slicks covering several km^2 of sea surface above these sites were reported earlier (Evtushenko and Ivanov, 2013; Körber et al., 2014) and were sampled for chemical analysis in this study. Similar to observations described for oil escaping the seafloor for instance in the Gulf of Mexico (Leifer and MacDonald, 2003), oil-gas bubbles disintegrated when reaching the sea-atmosphere boundary and non-volatile oily compounds remained on the sea surface, while volatiles escaped to the atmosphere. At Colkheti Seep the rising velocity of oil-covered gas bubbles released was estimated at 14 ± 1 cm s^{-1} close to the seafloor (Körber et al., 2014). Assuming a constant vertical velocity and negligible horizontal deflections, it would take a maximum of 133.3 min at Colkheti Seep (ca. 1,120 mbsl) and 121.4 min at Pechori Mound (ca. 1,020 mbsl), respectively, for intact oil–gas bubbles to float from the seafloor to the sea surface. A comparison of the composition of hydrocarbons extracted from oil in sediments at Colkheti Seep with those in the oil slick samples (Fig. 8) demonstrated that the heavily degraded oil remained relatively unaltered during passage through the predominantly anoxic Black Sea water column. Except for the early eluting compounds, which are prone to biodegradation, to water washing, and loss during laboratory workup, the "fingerprints" are similar and clearly support that oil slicks at the Colkheti Seep are sourced by close-by oil seepage at the seafloor. Relatively small differences in molecular compositions were already described for oil from the Maikop Group onshore Georgia and a slick-forming oil above Kobuleti Ridge (Dembicki, 2020) and also for oil migrating through the oxic water column in the Gulf of Mexico (MacDonald et al., 1993).

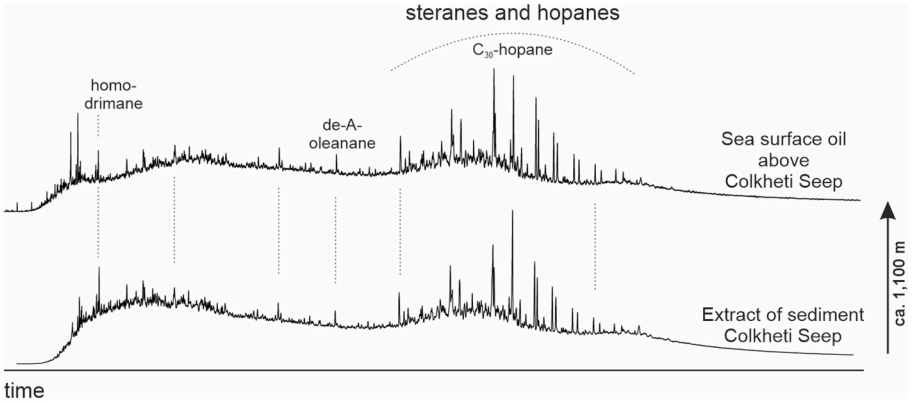

Fig. 8. Comparison of FID traces of hydrocarbons in oil extracted from sediments (53–56 cmbsf) recovered with pressure core GeoB14345 at Colkheti Seep (bottom) and a representative oil slick sample from the sea surface above Colkheti Seep (top). Mass spectrometric analyses revealed that the similar "fingerprints" represent identical compounds. For values see Table 3.

4.2.2. Low-molecular weight hydrocarbons

4.2.2.1. Alterations of light hydrocarbons in the methanogenic zone by microbial and physical transport processes. A nearly linear trend observed for the C_1/C_{2+} – $\delta^{13}C$–CH_4 data pairs at all sampling sites (Fig. 6a) suggests that the degree of biodegradation and variable mixture of secondary microbial hydrocarbons and of oil-associated thermogenic hydrocarbons is the major cause for the gas chemical differences observed (Milkov and Etiope; 2018). However, from the C_1/C_{2+} – $\delta^{13}C$–CH_4 relationships post-genetic advective migration of light hydrocarbons that are mostly reflected by modifications of molecular compositions rather than of carbon isotopic compositions (Etiope et al., 2009) cannot be completely ruled out. This process leads to a relative depletion in C_{2+} hydrocarbons, i.e. an increase in C_1/C_{2+} ratios (Leythaeuser et al., 1980; Milkov and Etiope, 2018; Schoell, 1983). Considering the steep slope between the data pairs, segregation during advective migration and/or mixing of hydrocarbon endmembers may be another process affecting the hydrocarbon composition at the four study sites. However, from our data set the individual impact of the aforementioned processes on the molecular and isotopic hydrocarbon compositions cannot be evaluated. Nevertheless, assuming that hydrocarbons seeping at the four sites investigated are likely generated from the same source rock(s), trends observed here would particularly reflect lowest effects of migration on hydrocarbons at the Pechori Mound and highest for those at the Batumi seep area. This assumption is corroborated by compressional uplift and severe faulting of overlying sediments underneath the tops of the gas and oil seeps and, in contrast, well defined sediment packages cut by vertical faults in the Batumi seep area as recorded previously (Bohrmann et al., 2007; Wagner-Friedrichs, 2007).

Biotic degradation of propane and *n*-butane in the subsurface has been proposed for vent gas discharged at the Batumi seep area (Pape et al., 2010). The 'natural gas plot' in Fig. 7 shows deviations towards more positive $\delta^{13}C$–C_3H_8 values indicative for removal of ^{12}C-enriched propane (or, more unlikely, secondary contribution of ^{13}C-enriched propane) at all sampling sites investigated in this study. Degradation of light hydrocarbons including propane within the methanogenic zone, might have been mediated by alkane-degrading bacteria using terminal electron acceptors other than sulfate (e.g., Stagars et al., 2016) and/or by sulfate-reducing bacteria in case of sulfate availability in the fueling hydrocarbon reservoir and/or on the long-distance migration pathway. For sedimentary gas within the sulfate-zone, the capability of sulfate-reducing bacteria to significantly degrade propane and *n*-butane (Kniemeyer et al., 2007) would additionally apply. For our sample set, strongest deviations from the line connecting $\delta^{13}C$ values of light hydrocarbons, i.e. enrichments in ^{13}C for propane, became obvious for samples from the Colkheti Seep and Pechori Mound (Fig. 7).

4.2.2.2. Modifications of volatile hydrocarbons in shallow sediments by microbial degradation and degassing. Ex situ concentrations of dissolved methane in the mM-range in uppermost sediments at the four studied sites substantiated strong hydrocarbon upward flux (Fig. 9a). Such cores originated from areas located close to seafloor gas emission sites and/or even contained gas hydrates (e.g., Batumi seep area – GeoB11904-15 (close to bubble hole); Iberia Mound – GeoB11938 (oil impregnations, gas hydrates); Colkheti Seep – GeoB11971 (oil, gas hydrates); Pechori Mound – GeoB11941 (oil)). In addition, cores taken from sites distant to seep sites were also characterized by relative methane depletions in comparably shallow depths and a shallow SMI.

In the following, we investigate molecular and isotopic compositions of light hydrocarbons obtained from short non-pressure cores (GrC, MUC, MIC) taken at each of the seeping areas (Fig. 9a–d). In order to asses modifications to the upward rising hydrocarbons in the course of early diagenesis we compare such hydrocarbon compositions with those determined for hydrate-bound gas and vent gas, as such gas types are considered less affected by geochemical transformation.

Light hydrocarbons in all gas types from each of the study sites displayed a dominance of methane with highest C_1/C_{2+} ratios at the Batumi seep area and lower ratios in the oil seep sediments and in particular at Pechori Mound (Fig. 9b). However, in comparison to $C_1/(C_2+C_3)$ ratios determined for light hydrocarbons from hydrate-bound gas and vent gas (highlighted by grey bars in Fig. 9b), those of gas from non-pressure cores were similar or slightly lower by trend. This is probably due to selective consumption of dissolved methane in the course of AOM (likely e.g., in GeoB11939 – Iberia Mound, GeoB11970 – Colkheti Seep (oil)) and/or to preferential loss of the most volatile hydrocarbon, methane, during recovery with the non-pressurized sampling tools.

Deviations from this general picture with increasing methane concentrations and increasing $C_1/(C_2+C_3)$ towards the sediment surface might result from lateral migration of hydrocarbons under high-flux conditions or methane de novo production (e.g., in GeoB11938 – Iberia Mound (gas hydrates, oil); GeoB11924 – Colkheti Seep (oil, gas hydrates); GeoB11941 – Pechori Mound (oil)). This interpretation is consistent with a very shallow, i.e. thin zone of AOM next to gas and oil emission sites caused by high fluid upward fluxes (Reitz et al., 2011).

$\delta^{13}C$ values of CH_4 and C_2H_6 in surface sediments recovered with the non-pressure tools (Fig. 9c, 9d) only slightly differed from those in hydrate-bound gas, vent gas and gas from pressure cores. Considerable negative excursions of $\delta^{13}C$–CH_4 values in concert with methane depletions were observed for sediments shallower than ca. 50 cmbsf from the Batumi seep area. This observation is commonly explained by carbon back-cycling in the course of AOM (e.g., Borowski, 2004). In contrast, $\delta^{13}C$–CH_4 and $\delta^{13}C$–C_2H_6 values in nearly all samples from the Iberia Mound, the Colkheti Seep and the Pechori Mound were similar to those measured in the respective hydrate and vent samples. These observations might reflect inefficient transformation of methane- and ethane-derived carbon at the three oil–gas seep sites.

5. Summary and Conclusions

1) A gas seepage area (Batumi seep area) and three oil-gas seepage sites (Iberia Mound, Colkheti Seep, Pechori Mound) located in the Eastern Black Sea were analyzed for the composition of oil and gas ascending from deeply buried sediments. Surface sediments of the Batumi seep area mainly contain hydrocarbons from organic matter deposited under recent anoxic conditions, while surface sediments at the three oil and gas seepages are additionally impregnated by migrated hydrocarbons.
2) A combination of various geochemical analytical techniques and organic geochemical indicators was applied in order to evaluate source rock, thermal maturity and biotic and abiotic modifications of oil and gas ascending through the sediment and through the water column.
3) Oil at the three oil-gas seepage sites is highly degraded and characterized by abundant unresolvable complex mixtures and the presence of tetra- and pentacyclic isoprenoids (mainly hopanes). It has most likely similar sources and is derived from a planktonic kerogen type with terrestrial contributions. Diagnostic isomerization patterns of hydrocarbons (e.g., steranes, hopanes) as well as stable carbon isotopic compositions of methane and ethane indicate that thermal maturities correspond to the early oil window.
4) Biomarker compositions and stable carbon isotope ratios of aliphatic hydrocarbons suggest similar source rock types for all four seep sites. The migrated hydrocarbons most likely originate from organic matter that has been deposited in an anoxic aquatic setting. Stable carbon isotopic ratios of hydrocarbon fractions along with the presence of the angiosperm biomarker oleanane indicate that the organic matter deposition took place after the Upper Cretaceous. The Eocene Kuma Formation and/or the Oligocene–Lower Miocene Maikop Group are the most likely sources for the majority of hydrocarbons generated.

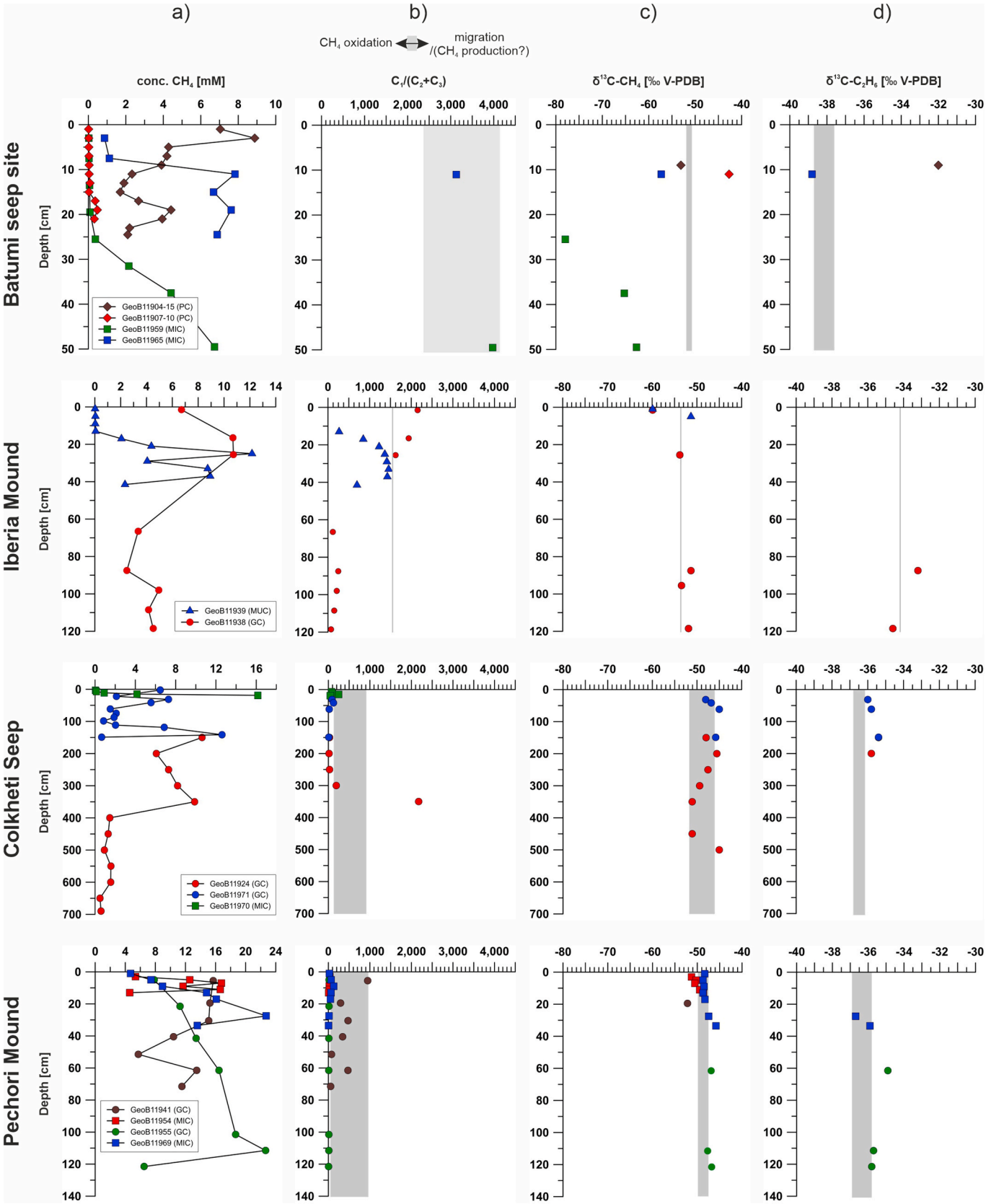

Fig. 9. Depth profiles of CH_4 concentrations (column 9a), $C_1/(C_2+C_3)$ values (column 9b) as well as $\delta^{13}C$–CH_4 (column 9c) and $\delta^{13}C$–C_2H_6 (column 9d) values in gas extracted from non-pressure sediment cores at the Batumi seep area (top line), Iberia Mound, Colkheti Seep and Pechori Mound (data adopted from Reitz et al., 2011) except for GeoB11970/-71). Grey lines and rectangles indicate ranges of values determined for hydrocarbons in hydrate-bound gas and vent gas sampled at the individual sites for comparison. Note different depth scales and CH_4 concentration ranges for individual sites. PC = Pushcore, MIC = Minicore, GrC = Gravity core, MUC = Multicore. Depth indications as centimeter core depth.

5) Molecular distribution patterns of light hydrocarbons (C_1–C_5) and stable carbon isotopic compositions of methane suggest that they are derived from both, oil-associated thermocatalytic processes and secondary microbial production from petroleum degradation. Large differences in C_1/C_{2+} but relatively small differences in $\delta^{13}C$–CH_4 between the individual study sites suggest that hydrocarbon mixtures consist of variable portions of admixed secondary microbial methane generated during petroleum degradation.
6) Oil-covered gas bubbles emitted from Pechori Mound and Colkheti Seep into the water column reach the sea-atmosphere boundary within less than 2.5 h and are not geochemically altered further during the passage. Oil and gas separate at the sea surface, leading to oil slick formation on the sea surface and gas escape into the atmosphere. Geochemical fingerprints demonstrate seeping oil at Colkheti Seep as distinct source for the floating oil slicks.

Credit author statement

Thomas Pape: Conceptualization, Investigation, Writing – original draft, Writing – review & editing, Visualization. Martin Blumenberg: Conceptualization, Investigation, Writing – original draft, Writing – review & editing, Visualization. Anja Reitz: Conceptualization, Investigation, Writing – original draft, Writing – review & editing. Georg Scheeder: Investigation, Writing – original draft, Writing – review & editing, Visualization. Mark Schmidt: Investigation, Writing – review & editing. Matthias Haeckel: Investigation, Writing – review & editing, Project administration, Funding acquisition. Valentina N. Blinova: Investigation, Writing – review & editing. Michael K. Ivanov: Investigation, Project administration, Funding acquisition. Heiko Sahling: Investigation, Project administration. Klaus Wallmann: Investigation, Writing – review & editing, Project administration, Funding acquisition. Gerhard Bohrmann: Investigation, Writing – review & editing, Supervision, Project administration, Funding acquisition.

Declaration of competing interest

The authors declare that they have no known competing financial interests or personal relationships that could have appeared to influence the work reported in this paper.

Acknowledgments

We are grateful to the masters, crews and shipboard parties of RV 'PROFESSOR LOGACHEV' (TTR-15), RV 'METEOR' (M72/3, M84/2), and RV 'MARIA S. MERIAN' (MSM15/2). The team of the remotely operated vehicle 'MARUM-QUEST 4000m' is thanked for excellent support during expeditions M72/3 and MSM15/2. We gratefully acknowledge K.-U. Hinrichs and V. Heuer (MARUM) for donation of sediment samples from TTR-15 cruise. H.-J. Hohnberg, K. Dehning, A.H. Mai, D. Hüttich (MARUM) are thanked for technical assistance with the DAPC system, and M. Weiβ, S. Kramer, A. Tietjen, and S. Koopmann (BGR) for laboratory work. T.P. thanks T. Malakhova (A.O. Kovalevsky Institute of Biology of the Southern Seas (IBSS), Sevastopol) for assistance with gas sampling and analysis during MSM15/2 and M84/2, respectively. P. Wintersteller (MARUM) is acknowledged for providing bathymetric map material and for sharing data on oil slick distributions on the sea surface and gas-oil rise velocities from the seafloor, respectively. B. Domeyer, A. Bleyer, R. Surberg, F. Scholz, D. Karaca, V. Mavromatis, and U. Lomnitz (GEOMAR) are thanked for sample preparation and analysis. Gabor C. Tari (OMV Exploration & Production GmbH, Vienna) and the special issue guest editor Katrin Schwalenberg (BGR) are thanked for their constructive comments that considerably helped to improve the manuscript.

Relevant data will be made publicly available through the World Data Center PANGAEA® (www.pangaea.de) after publication of this article. This study was funded by the German Ministry of Education and Research (BMBF) and the German Research Foundation (DFG), collaborative projects METRO (grant 03G0604A) and SUGAR (03SX320A + G), and through DFG-Research Center/Excellence Cluster 'The Ocean in the Earth System' (FZT 15). This paper is dedicated to Michael K. Ivanov (Moscow State University) and Heiko Sahling (MARUM) who were enthusiastic initiators of multilateral research on Marine Geoscience not only in the Black Sea.

APPENDIX A

Table A1
Specifics of sites and materials investigated in this study. Further information on sample characteristics can be found at the PANGAEA information system (Data Publisher for Earth & Environmental Science; https://www.pangaea.de/).

Site	Type of sample	Tool	Research cruise	Sample code	Lat	Long	Water Depth	Remarks (part of seafloor structure)	Study
				[GeoB]	[°N]	[°E]	[mbsl]		
Batumi seep area	Vent gas	GBS	M72/3	11904–16	41.9590	41.2902	833		*adopted from Pape et al. (2010)*
		GBS	M72/3	11907–2	41.9591	41.2922	834		*adopted from Pape et al. (2010)*
		GBS	M72/3	11907–5	41.9591	41.2912	835		*adopted from Pape et al. (2010)*
		GBS	M72/3	11919	41.9591	41.2888	833		*adopted from Pape et al. (2010)*
		GBS	M72/3	11921–1	41.9588	41.2878	844		*adopted from Pape et al. (2010)*
	Hydrate-bound gas	GrC	M72/3	11925	41.9572	41.2891	844		*adopted from Pape et al. (2010)*
		GrC	M72/3	11949	41.9592	41.2863	842		*adopted from Pape et al. (2010)*
		GrC	M72/3	11927	41.9568	41.2887	856		*adopted from Pape et al. (2010)*
		GrC	M72/3	11936	41.9593	41.2905	844		*adopted from Pape et al. (2010)*
		GrC	M72/3	11946	41.9589	41.2930	842		*adopted from Pape et al. (2010)*
		GrC	M72/3	11956	41.9575	41.2906	842		

(*continued on next page*)

Table A1 (*continued*)

Site	Type of sample	Tool	Research cruise	Sample code	Lat	Long	Water Depth	Remarks (part of seafloor structure)	Study
				[GeoB]	[°N]	[°E]	[mbsl]		
									adopted from Pape et al. (2010)
		GrC	M72/3	11975	41.9588	41.2931	844		*adopted from Pape et al. (2010)*
		GrC	M84/2	15236–1	41.9597	41.2902	838		*this study*
		GrC	M84/2	15249–1	41.9601	41.2877	842		*this study*
		GrC	M84/2	15251–1	41.9605	41.2847	842		*this study*
		GrC	M84/2	15260–1	41.9597	41.2899	839		*this study*
		MeBo	M84/2	15236–2	41.9598	41.2892	838		*this study*
	Sedimentary gas (pressure core)	DAPC	M72/3	11901	41.9568	41.2891	851		*adopted from Pape et al. (2010)*
		DAPC	M72/3	11903	41.9579	41.2878	850		*adopted from Pape et al. (2010)*
		DAPC	M72/3	11906	41.9578	41.2878	843		*adopted from Pape et al. (2010)*
		DAPC	M72/3	11918	41.9591	41.2905	840		*adopted from Pape et al. (2010)*
		DAPC	M72/3	11920	41.9576	41.2924	844		*adopted from Pape et al. (2010)*
		DAPC	M72/3	11937	41.9582	41.2910	842		*adopted from Pape et al. (2010)*
		DAPC	M72/3	11951	41.9591	41.2905	840		*adopted from Pape et al. (2010)*
		DAPC	M72/3	11958	41.9574	41.2908	847		*adopted from Pape et al. (2010)*
		DAPC	M72/3	11963	41.9568	41.2880	853		*adopted from Pape et al. (2010)*
	Sedimentary gas (non-pressurized)	PC	M72/3	11904–15	41.9590	41.2902	833	close to gas emission site	*this study*
		PC	M72/3	11907–10	41.9590	41.2902	833	close to gas emission site	*this study*
		MIC	M72/3	11959	41.9589	41.2928	840		*this study*
		MIC	M72/3	11965	41.9575	41.2906	843	at emission site	*this study*
	Sediment	GrC	TTR15	9909–1	41.9587	41.2930	856	Site 1	*this study*
		GrC	TTR15	9909–4	41.9587	41.2917	855	Site 2	*this study*
Iberia Mound	Hydrate-bound gas	GrC	M72/3	11938	41.8723	41.1673	982	oil-stained, gas hydrates	*this study*
	Sedimentary gas (non-pressurized)	GrC	M72/3	11938	41.8723	41.1673	982	oil-stained, gas hydrates	*adopted from Reitz et al. (2011)*
		MUC	M72/3	11939	41.8790	41.1671	989		*adopted from Reitz et al. (2011)*
Colkheti Seep	Vent gas	GBS	M72/3	11902–1	41.9679	41.1033	1,071		*this study*
	Hydrate-bound gas	GrC	TTR15	9931–1	41.9730	41.1023	1,142		*this study*
		GrC	M72/3	11923	41.9687	41.1042	1,088		*this study*
		GrC	M72/3	11924	41.9678	41.1033	1,056	oil-stained	*this study,*
		GrC	M72/3	11971	41.9678	41.1033	1,124	oil-stained	*this study*
	Sedimentary gas (pressure core)	DAPC	M72/3	11922	41.9679	41.1036	1,126	oil-stained	*this study*
		DAPC	MSM15/2	14345	41.9676	41.1032	1,129	oil-stained	*this study*
	Sedimentary gas (non-pressurized)	GrC	M72/3	11924	41.9678	41.1033	1,056	oil-stained, gas hydrates	*adopted from Reitz et al. (2011)*
		MIC	M72/3	11970	41.9678	41.1031	1,118		*this study*
		GrC	M72/3	11971	41.9678	41.1033	1,124	oil-stained, gas hydrates	*this study*
	Sediment	GrC	TTR15	9927–1	41.9730	41.1027	1,141	site 1	*this study*
	Oil slicks from sea surface (#2&3)		MSM15/2	not assigned					*this study*
Pechori Mound	Hydrate-bound gas	GrC	M72/3	11953	41.9824	41.1257	1,015		*this study*
		GrC	M72/3	11955	41.9827	41.1257	1,012	oil-stained	*this study*
		GrC	M84/2	15255	41.9816	41.1268	1,010	oil-stained	*this study*
		GrC	M84/2	15256	41.9823	41.1253	1,025		*this study*
		MeBo	M84/2	15227–1	41.9827	41.1266	1,025		*this study*
		MeBo	M84/2	15227–3	41.9831	41.1265	1,027		*this study*
	Sedimentary gas (non-pressurized)	GrC	M72/3	11941	41.9827	41.1234	1,014		*adopted from Reitz et al. (2011)*
		MIC	M72/3	11954	41.9827	41.1257	1,024	oil-stained	*adopted from Reitz et al. (2011)*
		GrC	M72/3	11955	41.9827	41.1257	1,012	oil-stained	*adopted from Reitz et al. (2011)*
		MIC	M72/3	11969	41.9827	41.1257	1,011		*adopted from Reitz et al. (2011)*
	Sediment	GrC	TTR15	9913–2	41.9833	41.1235	1,033	northwestern center	*this study*
		GrC	TTR15	9913–6	41.9833	41.1235	n.d.	northwestern center, oil-stained	*this study*
		GrC	TTR15	9913–1	41.9795	41.1265	1,045	southeastern rim	*this study*

GBS = Gas Bubble Sampler, DAPC = Dynamic Autoclave Piston Corer, GrC = Gravity Corer, MUC = Multicorer, MIC = Minicorer, MeBo = drill rig MARUM-MeBo70; TTR-15 = summer 2005, M72/3 = spring 2007, MSM15/2 = spring 2010, M84/2 = spring 2011; n.d. = not determined.

Table A2

Overview on analysis performed on organic extracts, fractions, and individual components.

Site	Preliminary sample code	Sample code	Sampling depth	Stable C isotopic compositions of hydrocarbon fractions	Hydrocarbon biomarkers (aliphatic fractions)	Gas composition	CH_4 concentrations	Stable H and C isotopic composition on volatiles
		[GeoB]	[cmbsf]	EA-IRMS	GC-MS	GC	GC	GC-IRMS
Batumi seep area	BS350	9909–1	324		X			
	BS353	9909–4	154		X			
		11904–15					X	X
		11907–10					X	
		11959				X		X
		11965				X		X
		15236–1				X		
		15249–1				X		
		15251–1				X		
		15260–1				X		
		15236–2				X		
Iberia Mound		11938				X	X	X
		11939				X	X	X
Colkheti Seep	BS374	9927–1	53–56	X	X			
	BS374	9927–1	80–83	X	X			
		11902–1				X		X
		11922				X		X
		11923				X		X
		11924				X	X	X
		11970				X	X	
		11971				X	X	X
		14345				X		X
	MSM15/2 -oil slick samples (#2&3)	not assigned			X			
Pechori Mound	BS355	9913–1	45–50	X	X			
	BS356	9913–2	43–46	X	X			
	BS360	9913–6	84–87	X	X			
		11941				X	X	X
		11955				X	X	X
		11969				X	X	X
		15227–1				X		
		15227–3				X		X
		15255				X		
		15256				X		

TOC = Total organic carbon; CNS = determination of carbon, nitrogen, and sulfur in sediments via flash combustion (N and S not considered in this study); EA-IRMS = Elemental analyzer- Isotope ratio mass spectrometry; GC-MS = Gas chromatography (GC) –mass spectrometry; GC-IRMS = Gas chromatography-Isotope ratio mass spectrometry.

References

Abegg, F., Hohnberg, H.J., Pape, T., Bohrmann, G., Freitag, J., 2008. Development and application of pressure-core-sampling systems for the investigation of gas- and gas-hydrate-bearing sediments. Deep-Sea Research I: Oceanographic Research Papers 55, 1590–1599. https://doi.org/10.1016/j.dsr.2008.06.006.

Abrams, M.A., Dahdah, N.F., Francu, E., 2009. Development of methods to collect and analyze gasoline range (C_5–C_{12}) hydrocarbons from seabed sediments as indicators of subsurface hydrocarbon generation and entrapment. Appl. Geochem. 24, 1951–1970. https://doi.org/10.1016/j.apgeochem.2009.07.009.

Abrams, M.A., Narimanov, A.A., 1997. Geochemical evaluation of hydrocarbons and their potential sources in the western South Caspian depression, Republic of Azerbaijan. Mar. Petrol. Geol. 14, 451–468. https://doi.org/10.1016/S0264-8172(97)00011-1.

Adamia, S., Alania, V., Chabukiani, A., Chichua, G., Enukidze, O., Sadradze, N., 2010. Evolution of the Late Cenozoic basins of Georgia (SW Caucasus): a review. In: Sosson, M., Kaymakci, N., Stephenson, R.A., Bergerat, F., Starostenko, V. (Eds.), Sedimentary Basin Tectonics from the Black Sea and Caucasus to the Arabian Platform. Geological Society, London, pp. 239–259. https://doi.org/10.1144/SP340.11.

Adamia, S., Zakariadze, G., Chkhotua, T., Sadradze, N., Tsereteli, N., Chabukiani, A., et al., 2011. Geology of the Caucasus: a review. Turk. J. Earth Sci. 20, 489–544. https://doi.org/10.3906/yer-1005-11.

Deep-water cold seeps, sedimentary environments and ecosystems of the Black and Tyrrhenian Sea and Gulf of Cadiz. In: Akhmetzhanov, A.M., Ivanov, M., Kenyon, N. H., Mazzini, A. (Eds.), 2007. IOC Technical Series No. 72. UNESCO, p. 99. http://hdl.handle.net/123456789/1428.

Artemov, Y.G., Egorov, V.N., Polikarpov, G.G., Gulin, S.B., 2007. Methane emission to the hydro- and atmosphere by gas bubble streams in the Dnieper Paleo-Delta, the Black Sea. Marine Ecological Journal 5, 5–26.

Bahr, A., Arz, H.W., Lamy, F., Wefer, G., 2006. Late glacial to Holocene paleoenvironmental evolution of the Black Sea, reconstructed with stable oxygen isotope records obtained on ostracod shells. Earth Planet Sci. Lett. 241, 863–875. https://doi.org/10.1016/j.epsl.2005.10.036.

Bahr, A., Pape, T., Abegg, F., Bohrmann, G., van Weering, T.C.E., Ivanov, M.K., 2010. Authigenic carbonates from the eastern Black Sea as an archive for shallow gas hydrate dynamics – results from the combination of CT imaging with mineralogical and stable isotope analyses. Mar. Petrol. Geol. 27, 1819–1829. https://doi.org/10.1016/j.marpetgeo.2010.08.005.

Banks, C.J., Robinson, A.G., Williams, A.P., 1997. Structure and regional tectonic of the Achara-Trialet Fold Belt and the adjacent Rioni and Kartli Foreland Basins, Republic of Georgia. In: Robinson, A.G. (Ed.), Regional and petroleum geology of the Black Sea and surrounding region. American Association of Petroleum Geologists, pp. 331–345.

Bechtel, A., Movsumova, U., Pross, J., Gratzer, R., Ćorić, S., Sachsenhofer, R.F., 2014. The Oligocene Maikop series of Lahich (eastern Azerbaijan): paleoenvironment and oil–source rock correlation. Org. Geochem. 71, 43–59. https://doi.org/10.1016/j.orggeochem.2014.04.005.

Beniamovski, V.N., Alekseev, A.S., Ovechkina, M.N., Oberhaensli, H., 2003. Middle to upper Eocene dysoxic-anoxic Kuma Formation (Northeast Peri-Tethys): Biostratigraphy and paleoenvironments. In: Wing, S.L., Gingerich, P.D., Schmitz, B., Thomas, E. (Eds.), Causes and consequences of globally warm climates in the early Paleogene, vol. 369. Geological Society of America, pp. 95–112.

Bernard, B.B., Brooks, J.M., Sackett, W.M., 1976. Natural gas seepage in the Gulf of Mexico. Earth Planet Sci. Lett. 31, 48–54. https://doi.org/10.1016/0012-821X(76)90095-9.

Bernard, B., Brooks, J.M., Sackett, W.M., 1977. A geochemical model for characterization of hydrocarbon gas sources in marine sediments. In: paper presented at Offshore Technology Conference, Offshore Technology Conference, Houston, Texas, 02.-05.05.1977. https://doi.org/10.4043/2934-ms.

Berner, U., Faber, E., 1988. Maturity related mixing model for methane, ethane and propane, based on carbon isotopes. Org. Geochem. 13, 67–72. https://doi.org/10.1016/B978-0-08-037236-5.50012-9.

Blumenberg, M., Seifert, R., Reitner, J., Pape, T., Michaelis, W., 2004. Membrane lipid patterns typify distinct anaerobic methanotrophic consortia. Proc. Natl. Acad. Sci. U. S. A 101, 11111–11116. https://doi.org/10.1073/pnas.0401188101.

Bohrmann, G., Akarsu, E., Bahr, A., Bergenthal, M., Dehning, K., Diekamp, V., et al., 2011. Report and preliminary results of RV METEOR Cruise M84/2, Istanbul – Istanbul, 26 February – 02 April, 2011. Origin and distribution of methane and methane hydrates in the Black Sea, Berichte. Fachbereich Geowissenschaften. Universität Bremen, Bremen, p. 164 urn:nbn:de:gbv:46-00102252-13.

Bohrmann, G., Ivanov, M., Foucher, J.-P., Spiess, V., Bialas, J., Greinert, J., et al., 2003. Mud volcanoes and gas hydrates in the Black Sea: new data from Dvurechenskii and Odessa mud volcanoes. Geo Mar. Lett. 23, 239–249. https://doi.org/10.1007/s00367-003-0157-7.

Bohrmann, G., Pape, T., cruise participants, 2007. Report and preliminary results of R/V Meteor cruise M72/3, Istanbul – Trabzon – Istanbul, 17 March – 23 April, 2007. Marine gas hydrates of the Eastern Black Sea. In: Bohrmann, G., Pape, T. (Eds.), Berichte, Fachbereich Geowissenschaften. Universität Bremen, No. 261, Bremen, p. 176.

Boote, D.R.D., Sachsenhofer, R.F., Tari, G., Arbouille, D., 2018. Petroleum provinces of the Paratethyan region. J. Petrol. Geol. 41, 247–297. https://doi.org/10.1111/jpg.12703.

Borowski, W.S., 2004. A review of methane and gas hydrates in the dynamic, stratified system of the Blake Ridge region, offshore southeastern North America. Chem. Geol. 205, 311–346. https://doi.org/10.1016/j.chemgeo.2003.12.022.

Burwicz, E., Haeckel, M., 2020. Basin-scale estimates on petroleum components generation in the Western Black Sea basin based on 3-D numerical modelling. Mar. Petrol. Geol. 113, 104122. https://doi.org/10.1016/j.marpetgeo.2019.104122.

Calvert, S.E., Karlin, R.E., 1998. Organic carbon accumulation in the Holocene sapropel of the Black Sea. Geology 26, 107–110. 10.1130/0091-7613(1998)026<0107:OCAITH>2.3.CO;2.

Chung, H.M., Gormly, J.R., Squires, R.M., 1988. Origin of gaseous hydrocarbons in subsurface environments: theoretical considerations of carbon isotope distribution. Chem. Geol. 71, 97–104. https://doi.org/10.1016/0009-2541(88)90108-8.

Claypool, G.E., Kvenvolden, K.A., 1983. Methane and other hydrocarbon gases in marine sediment. Annu. Rev. Earth Planet Sci. 11, 299–327. https://doi.org/10.1146/annurev.ea.11.050183.001503.

Cloetingh, S., Spadini, G., Van Wees, J.D., Beekman, F., 2003. Thermo-mechanical modelling of Black Sea Basin (de)formation. Sediment. Geol. 156, 169–184. https://doi.org/10.1016/S0037-0738(02)00287-7.

Dembicki Jr., Harry, 2020. Reducing the risk of finding a working petroleum system using SAR imaging, sea surface slick sampling, and geophysical seafloor characterization: an example from the eastern Black Sea basin, offshore Georgia. Mar. Petrol. Geol. 115, 104276. https://doi.org/10.1016/j.marpetgeo.2020.104276.

Dimitrov, L., 2002. Contribution to atmospheric methane by natural seepages on the Bulgarian continental shelf. Continent. Shelf Res. 22, 2429–2442. https://doi.org/10.1016/S0278-4343(02)00055-9.

Efendiyeva, M.A., 2004. Anoxia in waters of the Maikop paleobasin (Tethys Ocean, Azeri sector), with implications for the modern Caspian Sea. Geo Mar. Lett. 24, 177–181. https://doi.org/10.1007/s00367-004-0173-2.

Eglinton, G., Hamilton, R.J., Raphael, R.A., Gonzales, A.G., 1962. Hydrocarbon constituents of the wax coatings of plant leaves: a taxonomic study. Nature 193, 739–742. https://doi.org/10.1038/193739a0.

Ekweozor, C.M., Okogun, J.I., Ekong, D.E.U., Maxwell, J.R., 1979. Preliminary organic geochemical studies of samples from the Niger delta (Nigeria) I. Analyses of crude oils for triterpanes. Chem. Geol. 27, 11–28. https://doi.org/10.1016/0009-2541(79)90100-1.

Etiope, G., Feyzullayev, A., Milkov, A.V., Waseda, A., Mizobe, K., Sun, C.H., 2009. Evidence of subsurface anaerobic biodegradation of hydrocarbons and potential secondary methanogenesis in terrestrial mud volcanoes. Mar. Petrol. Geol. 26, 1692–1703. https://doi.org/10.1016/j.marpetgeo.2008.12.002.

Evtushenko, N.V., Ivanov, A.Y., 2013. Oil seeps in the southeastern Black Sea studied using satellite synthetic aperture radar images. Izvestiya Atmos. Ocean. Phys. 49, 913–918. https://doi.org/10.1134/s0001433813090065.

Faber, E., Schmidt, M., Feyzullayev, A., 2015. Geochemical hydrocarbon exploration – insights from stable isotope models. Oil Gas Eur. Mag. 41, 93–98.

Formolo, M.J., Lyons, T.W., Zhang, C.L., Kelley, C., Sassen, R., Horita, J., et al., 2004. Quantifying carbon sources in the formation of authigenic carbonates at gas hydrate sites in the Gulf of Mexico. Chem. Geol. 205, 253–264. https://doi.org/10.1016/j.chemgeo.2003.12.021.

Greinert, J., Artemov, Y., Egorov, V., De Batist, M., McGinnis, D., 2006. 1300-m-high rising bubbles from mud volcanoes at 2080 m in the Black Sea: hydroacoustic characteristics and temporal variability. Earth Planet Sci. Lett. 244, 1–15. https://doi.org/10.1016/j.epsl.2006.02.011.

Haeckel, M., Reitz, A., Klaucke, I., 2008. Methane budget of a large gas hydrate province offshore Georgia, Black Sea. In: paper presented at 6th International Conference on Gas hydrates (ICGH 2008), Vancouver, British Columbia, 06.-10.07.2008..

Head, I.M., Jones, D.M., Larter, S.R., 2003. Biological activity in the deep subsurface and the origin of heavy oil. Nature 426, 344–352. https://doi.org/10.1038/nature02134.

Heeschen, K., Haeckel, M., Klaucke, I., Ivanov, M.K., Bohrmann, G., 2011. Quantifying in-situ gas hydrates at active seep sites in the eastern Black Sea using pressure coring technique. BGeo 8, 3555–3565. https://doi.org/10.5194/bg-8-3555-2011.

Heeschen, K.U., Hohnberg, H.J., Haeckel, M., Abegg, F., Drews, M., Bohrmann, G., 2007. In situ hydrocarbon concentrations from pressurized cores in surface sediments, Northern Gulf of Mexico. Mar. Chem. 107, 498–515. https://doi.org/10.1016/j.marchem.2007.08.008.

Huang, W.-Y., Meinschein, W.G., 1979. Sterols as ecological indicators. Geochem. Cosmochim. Acta 43, 739–745. https://doi.org/10.1016/0016-7037(79)90257-6.

Hunt, J.M., 1996. Petroleum Geochemistry and Geology, second ed. W.H. Freeman, p. 743.

Inan, S., Namik Yalçin, M., Guliev, I.S., Kuliev, K., Akper Feizullayev, A., 1997. Deep petroleum occurrences in the Lower Kura Depression, South Caspian Basin, Azerbaijan: an organic geochemical and basin modeling study. Mar. Petrol. Geol. 14, 731–762. https://doi.org/10.1016/S0264-8172(97)00058-5.

Kessler, J.D., Reeburgh, W.S., Southon, J., Seifert, R., Michaelis, W., Tyler, S.C., 2006. Basin-wide estimates of the input of methane from seeps and clathrates to the Black Sea. Earth Planet Sci. Lett. 243, 366–375. https://doi.org/10.1016/j.epsl.2006.01.006.

Killops, S., Killops, V., 2013. An Introduction to Organic Geochemistry, second ed. Blackwell Science, p. 404.

Klaucke, I., Sahling, H., Bürk, D., Weinrebe, W., Bohrmann, G., 2005. Mapping deep-water gas emissions with sidescan sonar. EOS, Transactions 86, 341–352. https://doi.org/10.1029/2005EO380002.

Klaucke, I., Sahling, H., Weinrebe, W., Blinova, V., Bürk, D., Lursmanashvili, N., et al., 2006. Acoustic investigation of cold seeps offshore Georgia, eastern Black Sea. Mar. Geol. 231, 51–67. https://doi.org/10.1016/j.margeo.2006.05.011.

Kniemeyer, O., Musat, F., Sievert, S.M., Knittel, K., Wilkes, H., Blumenberg, M., et al., 2007. Anaerobic oxidation of short-chain hydrocarbons by marine sulphate-reducing bacteria. Nature 449, 898–901. https://doi.org/10.1038/nature06200.

Körber, J.-H., Sahling, H., Pape, T., dos Santos Ferreira, C., MacDonald, I., Bohrmann, G., 2014. Natural oil seepage at Kobuleti Ridge, eastern Black Sea. Mar. Petrol. Geol. 50, 68–82. https://doi.org/10.1016/j.marpetgeo.2013.11.007.

Kruglyakova, R.P., Byakov, Y.A., Kruglyakova, M.V., Chalenko, L.A., Shevtsova, N.T., 2004. Natural oil and gas seeps on the Black Sea floor. Geo Mar. Lett. 24, 150–162. https://doi.org/10.1007/s00367-004-0171-4.

Leifer, I., MacDonald, I., 2003. Dynamics of the gas flux from shallow gas hydrate deposits: interaction between oily hydrate bubbles and the oceanic environment. Earth Planet Sci. Lett. 210, 411–424. https://doi.org/10.1016/S0012-821X(03)00173-0.

Leythaeuser, D., Schaefer, R.G., Yukler, A., 1980. Diffusion of light hydrocarbons through near-surface rocks. Nature 284, 522–525. https://doi.org/10.1038/284522a0.

MacDonald, I.R., Guinasso Jr., N.L., Ackleson, S.G., Amos, J.F., Duckworth, R., Sassen, R., et al., 1993. Natural oil slicks in the Gulf of Mexico visible from space. J. Geophys. Res. 98, 16351–16364. https://doi.org/10.1029/93jc01289.

Mayer, J., Rupprecht, B.J., Sachsenhofer, R.F., Tari, G., Bechtel, A., Coric, S., et al., 2018a. Source potential and depositional environment of Oligocene and Miocene rocks offshore Bulgaria. Geological Society, London, Special Publications 464, 307–328. https://doi.org/10.1144/sp464.2.

Mayer, J., Sachsenhofer, R.F., Ungureanu, C., Bechtel, A., Gratzer, R., Sweda, M., et al., 2018b. Petroleum charge and migration in the Black Sea: insights from oil and source rock geochemistry. J. Petrol. Geol. 41, 337–350. https://doi.org/10.1111/jpg.12706.

Michaelis, W., Seifert, R., Nauhaus, K., Treude, T., Thiel, V., Blumenberg, M., et al., 2002. Microbial reefs in the Black Sea fueled by anaerobic oxidation of methane. Science 297, 1013–1015. https://doi.org/10.1126/science.1072502.

Milkov, A.V., 2011. Worldwide distribution and significance of secondary microbial methane formed during petroleum biodegradation in conventional reservoirs. Org. Geochem. 42, 184–207. https://doi.org/10.1016/j.orggeochem.2010.12.003.

Milkov, A.V., Etiope, G., 2018. Revised genetic diagrams for natural gases based on a global dataset of >20,000 samples. Org. Geochem. 125, 109–120. https://doi.org/10.1016/j.orggeochem.2018.09.002.

Minshull, T.A., Keddie, A., 2010. Measuring the geotherm with gas hydrate bottom-simulating reflectors: a novel approach using three-dimensional seismic data from the eastern Black Sea. Terra. Nova 22, 131–136. https://doi.org/10.1111/j.1365-3121.2010.00926.x.

Moldowan, J.M., Dahl, J., Huizinga, B.J., Fago, F.J., Hickey, L.J., Peakman, T.M., et al., 1994. The molecular fossil record of oleanane and its relation to angiosperms. Science 265, 768–771. https://doi.org/10.1126/science.265.5173.768.

Monteleone, V., Minshull, T.A., Marin-Moreno, H., 2019. Spatial and temporal evolution of rifting and continental breakup in the eastern Black Sea basin revealed by long-offset seismic reflection data. Tectonics 38, 2646–2667. https://doi.org/10.1029/2019tc005523.

Naudts, L., Greinert, J., Artemov, Y., Staelens, P., Poort, J., Van Rensbergen, P., et al., 2006. Geological and morphological setting of 2778 methane seeps in the Dnepr paleo-delta, northwestern Black Sea. Mar. Geol. 227, 177–199. https://doi.org/10.1016/j.margeo.2005.10.005.

Nikishin, A.M., Korotaev, M.V., Ershov, A.V., Brunet, M.-F., 2003. The Black Sea basin: tectonic history and Neogene-Quaternary rapid subsidence modelling. Sediment. Geol. 156, 149–168. https://doi.org/10.1016/S0037-0738(02)00286-5.
Nikishin, A.M., Okay, A.I., Tüysüz, O., Demirer, A., Amelin, N., Petrov, E., 2015a. The Black Sea basins structure and history: new model based on new deep penetration regional seismic data. Part 1: basins structure and fill. Mar. Petrol. Geol. 59, 638–655. https://doi.org/10.1016/j.marpetgeo.2014.08.017.
Nikishin, A.M., Okay, A., Tüysüz, O., Demirer, A., Wannier, M., Amelin, N., et al., 2015b. The Black Sea basins structure and history: new model based on new deep penetration regional seismic data. Part 2: tectonic history and paleogeography. Mar. Petrol. Geol. 59, 656–670. https://doi.org/10.1016/j.marpetgeo.2014.08.018.
Nikolovska, A., Sahling, H., Bohrmann, G., 2008. Novel hydro-acoustic methodology for detection, localization and quantification of gas bubbles rising from the seafloor at gas seeps from the eastern Black Sea. G-cubed 9, Q10010. https://doi.org/10.1029/2008GC002118.
Okay, A.I., Celal Şengör, A.M., Görür, N., 1994. Kinematic history of the opening of the Black Sea and its effect on the surrounding regions. Geology 22, 267–270. https://doi.org/10.1130/0091-7613(1994)022<0267:khotoo>2.3.co;2.
Özsoy, E., Ünlüata, Ü., 1997. Oceanography of the Black Sea: a review of some recent results. Earth Sci. Rev. 42, 231–272. https://doi.org/10.1016/S0012-8252(97)81859-4.
Pape, T., Bahr, A., Klapp, S.A., Abegg, F., Bohrmann, G., 2011. High-intensity gas seepage causes rafting of shallow gas hydrates in the southeastern Black Sea. Earth Planet Sci. Lett. 307, 35–46. https://doi.org/10.1016/j.epsl.2011.04.030.
Pape, T., Bahr, A., Rethemeyer, J., Kessler, J.D., Sahling, H., Hinrichs, K.U., et al., 2010. Molecular and isotopic partitioning of low-molecular weight hydrocarbons during migration and gas hydrate precipitation in deposits of a high-flux seepage site. Chem. Geol. 269, 350–363. https://doi.org/10.1016/j.chemgeo.2009.10.009.
Pape, T., Haeckel, M., Riedel, M., Kölling, M., Schmidt, M., Wallmann, K., et al., 2020. This issue. Formation pathways of light hydrocarbons in deep sediments of the Danube deep-sea fan, Western Black Sea. Mar. Petrol. Geol. 122, 104627. https://doi.org/10.1016/j.marpetgeo.2020.104627.
Pedersen, T.F., Calvert, S.E., 1990. Anoxia vs. productivity: what controls the formation of organic-carbon-rich sediments and sedimentary rocks? AAPG Bull. 74, 454–466. https://doi.org/10.1306/0C9B232B-1710-11D7-8645000102C1865D.
Peters, K.E., Walters, C.C., Moldowan, J.M., 2004. The Biomarker Guide: Volume 2, Biomarkers and Isotopes in Petroleum Systems and Earth History. The Press Syndicate of the University of Cambridge, Cambridge, p. 704.
Pupp, M., Bechtel, A., Ćorić, S., Gratzer, R., Rustamov, J., Sachsenhofer, R.F., 2018. Eocene and Oligo-Miocene source rocks in the Rioni and Kura basins of Georgia: depositional environemtn and petroleum potential. J. Petrol. Geol. 41, 367–392. https://doi.org/10.1111/jpg.12708.
Quigley, T.M., Mackenzie, A.S., 1988. The temperatures of oil and gas formation in the sub-surface. Nature 333, 549. https://doi.org/10.1038/333549a0.
Reeburgh, W.S., Ward, B.B., Whalen, S.C., Sandbeck, K.A., Kilpatrick, K.A., Kerkhof, L.J., 1991. Black Sea methane geochemistry. Deep Sea Res. 38, S1189–S1210. https://doi.org/10.1016/S0198-0149(10)80030-5.
Reitz, A., Pape, T., Haeckel, M., Schmidt, M., Berner, U., Scholz, F., et al., 2011. Sources of fluids and gases expelled at cold seeps offshore Georgia, eastern Black Sea. Geochem. Cosmochim. Acta 75, 3250–3268. https://doi.org/10.1016/j.gca.2011.03.018.
Riboulot, V., Ker, S., Sultan, N., Thomas, Y., Marsset, B., Scalabrin, C., et al., 2018. Freshwater lake to salt-water sea causing widespread hydrate dissociation in the Black Sea. Nat. Commun. 9, 117. https://doi.org/10.1038/s41467-017-02271-z.
Riva, A., Caccialanza, P.G., Quagliaroli, F., 1988. Recognition of 18β (H)oleanane in several crudes and Tertiary-Upper Cretaceous sediments. Definition of a new maturity parameter. Org. Geochem. 13, 671–675. https://doi.org/10.1016/0146-6380(88)90088-5.
Robinson, A.G. (Ed.), 1997. Regional and Petroleum Geology of the Black Sea and Surrounding Region. American Association of Petroleum Geologists, p. 385.
Robinson, A.G., Rudat, J.H., Banks, C.J., Wiles, R.L.F., 1996. Petroleum geology of the Black Sea. Mar. Petrol. Geol. 13, 195–223.
Römer, M., Sahling, H., dos Santos Ferreira, C., Bohrmann, G., 2020. Methane gas emissions of the Black Sea—mapping from the Crimean continental margin to the Kerch Peninsula slope. Geo Mar. Lett. 40, 467–480. https://doi.org/10.1007/s00367-019-00611-0.
Römer, M., Sahling, H., Pape, T., Bahr, A., Feseker, T., Wintersteller, P., et al., 2012. Geological control and magnitude of methane ebullition from a high-flux seep area in the Black Sea—the Kerch seep area. Mar. Geol. 319–322, 57–74. https://doi.org/10.1016/j.margeo.2012.07.005.
Ross, D.A., Degens, E.T., 1974. Recent sediments of the Black Sea. In: Degens, E.T., Ross, D.A. (Eds.), The Black Sea – Geology, Chemistry and Biology. American Association of Petroleum Geologists, Tusla, USA, pp. 183–199.
Sachsenhofer, R.F., Popov, S.V., Akhmetiev, M.A., Bechtel, A., Gratzer, R., Groß, D., et al., 2017. The type section of the Maikop Group (Oligocene-lower Miocene) at the Belaya River (North Caucasus): Depositional environment and hydrocarbon potential. AAPG Bull. 101, 289–319.
Sachsenhofer, R.F., Popov, S.V., Bechtel, A., Coric, S., Francu, J., Gratzer, R., et al., 2018a. Oligocene and Lower Miocene source rocks in the Paratethys: palaeogeographical and stratigraphic controls. Geological Society, London, Special Publications 464, 267–306. https://doi.org/10.1144/sp464.1.
Sachsenhofer, R.F., Popov, S.V., Coric, S., Mayer, J., Misch, D., Morton, M.T., et al., 2018b. Paratethyan petroleum source rocks: an overview. J. Petrol. Geol. 41, 219–245. https://doi.org/10.1111/jpg.12702.
Sahling, H., Bohrmann, G., Artemov, Y.G., Bahr, A., Brüning, M., Klapp, S.A., et al., 2009. Vodyanitskii mud volcano, Sorokin trough, Black Sea: geological characterization and quantification of gas bubble streams. Mar. Petrol. Geol. 26, 1799–1811. https://doi.org/10.1016/j.marpetgeo.2009.01.010.
Schmale, O., Greinert, J., Rehder, G., 2005. Methane emission from high-intensity marine gas seeps in the Black Sea into the atmosphere. Geophys. Res. Lett. 32, L07609. https://doi.org/10.1029/2004GL021138.
Schmale, O., Haeckel, M., McGinnis, D.F., 2011. Response of the Black Sea methane budget to massive short-term submarine inputs of methane. BGeo 8, 911–918. https://doi.org/10.5194/bgd-7-9117-2010.
Schoell, M., 1983. Genetic characterization of natural gases. AAPG Bull. 67, 2225–2238. https://doi.org/10.1306/AD46094A-16F7-11D7-8645000102C1865D.
Schoell, M., 1988. Multiple origins of methane in the earth. Chem. Geol. 71, 1–10. https://doi.org/10.1016/0009-2541(88)90101-5.
Seewald, J.S., 2003. Organic-inorganic interactions in petroleum-producing sedimentary basins. Nature 426, 327–333. https://doi.org/10.1038/nature02132.
Seifert, W., Moldowan, J.M., 1980. The effect of thermal stress on source-rock quality as measured by hopane stereochemistry. Phys. Chem. Earth 12, 229–237. https://doi.org/10.1016/0079-1946(79)90107-1.
Seifert, W.K., Moldowan, J.M., 1986. Use of biological markers in petroleum exploration. In: Johns, R.B. (Ed.), Methods in Geochemistry and Geophysics, vol. 24, pp. 261–290.
Shillington, D.J., White, N., Minshull, T.A., Edwards, G.R.H., Jones, S.M., Edwards, R.A., et al., 2008. Cenozoic evolution of the eastern Black Sea: a test of depth-dependent stretching models. Earth Planet Sci. Lett. 265, 360–378. https://doi.org/10.1016/j.epsl.2007.10.033.
Shillington, D.J., Minshull, T.A., Edwards, R.A., White, N., 2018. Crustal structure of the mid Black Sea high from wide-angle seismic data. Geological Society, London, Special Publications 464, 19–32. https://doi.org/10.1144/sp464.6.
Shipboard Scientific Party, 1996. Explanatory notes. In: Paull, C.K., Matsumoto, R., Wallace, P.J. (Eds.), Proc. ODP, Init. Rept. Ocean Drilling Program, College Station, TX, pp. 13–41.
Sipahioglu, N.O., Karahanoglu, N., Altiner, D., 2013. Analysis of Plio-Quaternary deep marine systems and their evolution in a compressional tectonic regime, Eastern Black Sea Basin. Mar. Petrol. Geol. 43, 187–207. https://doi.org/10.1016/j.marpetgeo.2013.02.008.
Sofer, Z., 1984. Stable carbon isotope compositions of crude oils: application to source depositional environments and petroleum alteration. AAPG Bull. 68, 31–49. https://doi.org/10.1306/AD460963-16F7-11D7-8645000102C1865D.
Soulet, G., Ménot, G., Lericolais, G., Bard, E., 2011. A revised calendar age for the last reconnection of the Black Sea to the global ocean. QSRv 30, 1019–1026. https://doi.org/10.1016/j.quascirev.2011.03.001.
Stagars, M.H., Ruff, S.E., Amann, R., Knittel, K., 2016. High diversity of anaerobic alkane-degrading microbial communities in marine seep sediments based on (1-methylalkyl)succinate synthase genes. Front. Microbiol. 6 https://doi.org/10.3389/fmicb.2015.01511.
Starostenko, V., Buryanov, V., Makarenko, I., Rusakov, O., Stephenson, R., Nikishin, A., et al., 2004. Topography of the crust-mantle boundary beneath the Black Sea basin. Tectonophysics 381, 211–233. https://doi.org/10.1016/j.tecto.2002.08.001.
Stephenson, R., Schellart, W., 2010. The Black Sea back-arc basin: insights to its origin from geodynamic models of modern analogues. In: Kaymakci, M., Stephenson, R.A., Bergerat, F., Starostenko, V.I. (Eds.), Sedimentary Basin Tectonics from the Black Sea and Caucasus to the Arabian Platform. Geological Society of London, special Publications, pp. 11–21. https://doi.org/10.1144/SP340.2.
Tari, G., Vakhania, D., Tatishvili, G., Mikeladze, V., Gogritchiani, K., Vacharadze, S., et al., 2018. Stratigraphy, structure and petroleum exploration play types of the Rioni Basin, Georgia. Geological Society, London, Special Publications 464. https://doi.org/10.1144/sp464.14.
Tari, G.C., Simmons, M.D., 2018. History of deepwater exploration in the Black Sea and an overview of deepwater petroleum play types. Geological Society, London, Special Publications 464. https://doi.org/10.1144/sp464.16.
Tobias, H.J., Brenna, J.T., 1997. On-line pyrolysis as a limitless reduction source for high-precision isotopic analysis of organic-derived hydrogen. Anal. Chem. 69, 3148–3152. https://doi.org/10.1021/ac970332v.
Treude, T., Orphan, V., Knittel, K., Gieseke, A., House, C.H., Boetius, A., 2007. Consumption of methane and CO_2 by methanotrophic microbial mats from gas seeps of the anoxic Black Sea. Appl. Environ. Microbiol. 73, 2271–2283. https://doi.org/10.1128/aem.02685-06.
Vassilev, A., Dimitrov, L., 2002. Spatial and quantity evaluation of the Black Sea gas hydrates. Russ. Geol. Geophys. 43, 672–684.
Vincent, S.J., Braham, W., Lavrishchev, V.A., Maynard, J.R., Harland, M., 2016. The formation and inversion of the western Greater Caucasus Basin and the uplift of the western Greater Caucasus: Implications for the wider Black Sea region. Tectonics 35, 2948–2962. https://doi.org/10.1002/2016tc004204.
Vincent, S.J., Kaye, M.N.D., 2018. Source rock evaluation of Middle Eocene–Early Miocene mudstones from the NE margin of the Black Sea. Geological Society, London, Special Publications 464, 329–363. https://doi.org/10.1144/sp464.7.
Vincent, S.J., Morton, A.C., Carter, A., Gibbs, S., Barabadze, T.G., 2007. Oligocene uplift of the Western Greater Caucasus: an effect of initial Arabia–Eurasia collision. Terra. Nova 19, 160–166. https://doi.org/10.1111/j.1365-3121.2007.00731.x.
Wagner-Friedrichs, M., 2007. Seafloor seepage in the Black Sea: mud volcanoes, seeps and diapiric structures imaged by acoustic methods. Ph.D. thesis. University of Bremen, Bremen, p. 154.
Wakeham, S.G., Amann, R., Freeman, K.H., Hopmans, E.C., Jorgensen, B.B., Putnam, I.F., et al., 2007. Microbial ecology of the stratified water column of the Black Sea as revealed by a comprehensive biomarker study. Org. Geochem. 38, 2070–2097. https://doi.org/10.1016/j.orggeochem.2007.08.003.

Whiticar, M.J., 1999. Carbon and hydrogen isotope systematics of bacterial formation and oxidation of methane. Chem. Geol. 161, 291–314. https://doi.org/10.1016/S0009-2541(99)00092-3.

Wilhelms, A., Larter, S.R., Head, I., Farrimond, P., di-Primio, R., Zwach, C., 2001. Biodegradation of oil in uplifted basins prevented by deep-burial sterilization. Nature 411, 1034–1037. https://doi.org/10.1038/35082535.

Zander, T., Haeckel, M., Klaucke, I., Bialas, J., Klaeschen, D., Papenberg, C., et al., 2020. This issue. New insights into geology and geochemistry of the Kerch seep area in the Black Sea. Mar. Petrol. Geol. 113, 104162. https://doi.org/10.1016/j.marpetgeo.2019.104162.

Zonenshain, L.P., Pichon, X., 1986. Deep basins of the Black Sea and Caspian Sea as remnants of mesozoic back-arc basins. Tectonophysics 123, 181–211. https://doi.org/10.1016/0040-1951(86)90197-6.